Article

Cell Reports

Distinct Corticostriatal GABAergic Neurons Modulate Striatal Output Neurons and Motor Activity

Graphical Abstract

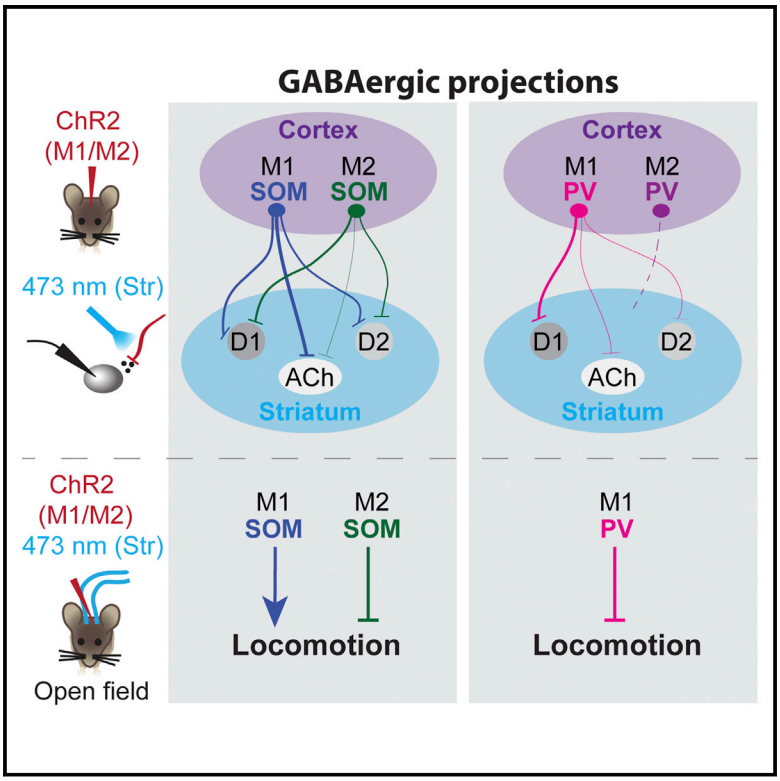

Authors

Sarah Melzer, Mariana Gil, David E. Koser, Magdalena Michael, Kee Wui Huang, Hannah Monyer

Correspondence

h.monyer@dkfz-heidelberg.de

In Brief

Melzer et al. characterize two cytochemically distinct GABAergic projecting neurons from the motor cortex to the dorsal striatum. These distinct populations of motor cortex GABAergic projecting neurons differentially innervate striatal neurons and differentially modulate motor activity.

Highlights

- Long-range GABAergic projections from the motor cortex directly innervate the striatum
- M1 and M2 long-range SOM$^+$ and PV$^+$ neurons differentially innervate striatal neurons
- Striatal cholinergic neurons are innervated mainly by M1 SOM$^+$ projecting neurons
- Motor cortex PV$^+$ and SOM$^+$ projecting neurons differentially modulate locomotion

Melzer et al., 2017, Cell Reports *19*, 1045–1055
May 2, 2017
http://dx.doi.org/10.1016/j.celrep.2017.04.024

Cell Reports
Article

Distinct Corticostriatal GABAergic Neurons Modulate Striatal Output Neurons and Motor Activity

Sarah Melzer,[1,3,4] Mariana Gil,[1,3] David E. Koser,[1] Magdalena Michael,[1] Kee Wui Huang,[2] and Hannah Monyer[1,5,*]
[1]Department of Clinical Neurobiology at the Medical Faculty of Heidelberg University and German Cancer Research Center (DKFZ), Im Neuenheimer Feld 280, 69120 Heidelberg, Germany
[2]Department of Neurobiology, Howard Hughes Medical Institute, Harvard Medical School, 220 Longwood Avenue, Boston, MA 02115, USA
[3]These authors contributed equally
[4]Present address: Department of Neurobiology, Howard Hughes Medical Institute, Harvard Medical School, 220 Longwood Avenue, Boston, MA 02115, USA
[5]Lead Contact
*Correspondence: h.monyer@dkfz-heidelberg.de
http://dx.doi.org/10.1016/j.celrep.2017.04.024

SUMMARY

The motor cortico-basal ganglion loop is critical for motor planning, execution, and learning. Balanced excitation and inhibition in this loop is crucial for proper motor output. Excitatory neurons have been thought to be the only source of motor cortical input to the striatum. Here, we identify long-range projecting GABAergic neurons in the primary (M1) and secondary (M2) motor cortex that target the dorsal striatum. This population of projecting GABAergic neurons comprises both somatostatin-positive (SOM$^+$) and parvalbumin-positive (PV$^+$) neurons that target direct and indirect pathway striatal output neurons as well as cholinergic interneurons differentially. Notably, optogenetic stimulation of M1 PV$^+$ and M2 SOM$^+$ projecting neurons reduced locomotion, whereas stimulation of M1 SOM$^+$ projecting neurons enhanced locomotion. Thus, corticostriatal GABAergic projections modulate striatal output and motor activity.

INTRODUCTION

The striatum is the primary input area of the basal ganglia. It integrates signals from cortical areas and subserves important functions like motor control (Tecuapetla et al., 2014; Kravitz et al., 2010) and reinforcement/punishment coding (Kravitz et al., 2012). Striatal neurons comprise GABAergic spiny projection neurons (SPNs, 95%) and interneurons (5%). SPNs are classified into direct pathway SPNs (dSPNs), which project to the substantia nigra reticulata and external and internal segments of the globus pallidus (GPe and GPi, respectively), and indirect pathway SPNs (iSPNs), which project to GPe (Bolam et al., 2000; Wu et al., 2000). Striatal interneurons include large aspiny cholinergic neurons and different populations of GABAergic interneurons (Kawaguchi et al., 1995).

Excitatory glutamatergic neurons from virtually all cortical areas send projections to the striatum (McGeorge and Faull, 1989), and several studies suggest their recruitment during action selection (Xiong et al., 2015; Znamenskiy and Zador, 2013; Koralek et al., 2012). In contrast, cortical GABAergic neurons projecting to the striatum were not considered to be a component of the canonical corticostriatal network because they were identified only in the prefrontal, somatosensory, and retrosplenial cortices (Lee et al., 2014; Jinno and Kosaka, 2004). Only recently were direct GABAergic neurons projecting to the striatum also described in the motor and auditory cortices (Rock et al., 2016). The authors identified the long-range projecting neurons as somatostatin-positive (SOM$^+$) and, furthermore, reported that inhibition conveyed by these neurons was onto both dSPNs and iSPNs. We previously showed that long-range GABAergic neurons connecting several brain structures comprise different molecular subtypes. For instance, connectivity between the hippocampus and medial entorhinal cortex is supported by parvalbumin-positive (PV$^+$) and SOM$^+$ neurons (Melzer et al., 2012). Moreover, projections from the septum to the medial entorhinal cortex are PV$^+$ and Calbindin$^+$, and they inhibit specific interneurons differentially (Fuchs et al., 2016). Hence, we wondered whether long-range GABAergic projecting neurons from the motor cortex to the striatum are diverse with respect to their molecular identity, target specificity, and function at the behavioral level.

Based on virus-mediated tracing, optogenetics, patch-clamp recordings in vitro, and behavioral essays, we identified two distinct populations of long-range projecting GABAergic neurons in the primary (M1) and secondary (M2) motor cortex targeting the dorsal striatum and established that these two populations exhibit target cell preference in the striatum and affect locomotion differentially.

RESULTS

Motor Cortex Long-Range Projecting SOM$^+$ Neurons Target the Striatum

SOM$^+$ cells are a major source of intracortical and corticofugal long-range GABAergic projections (Tomioka et al., 2005; Rock

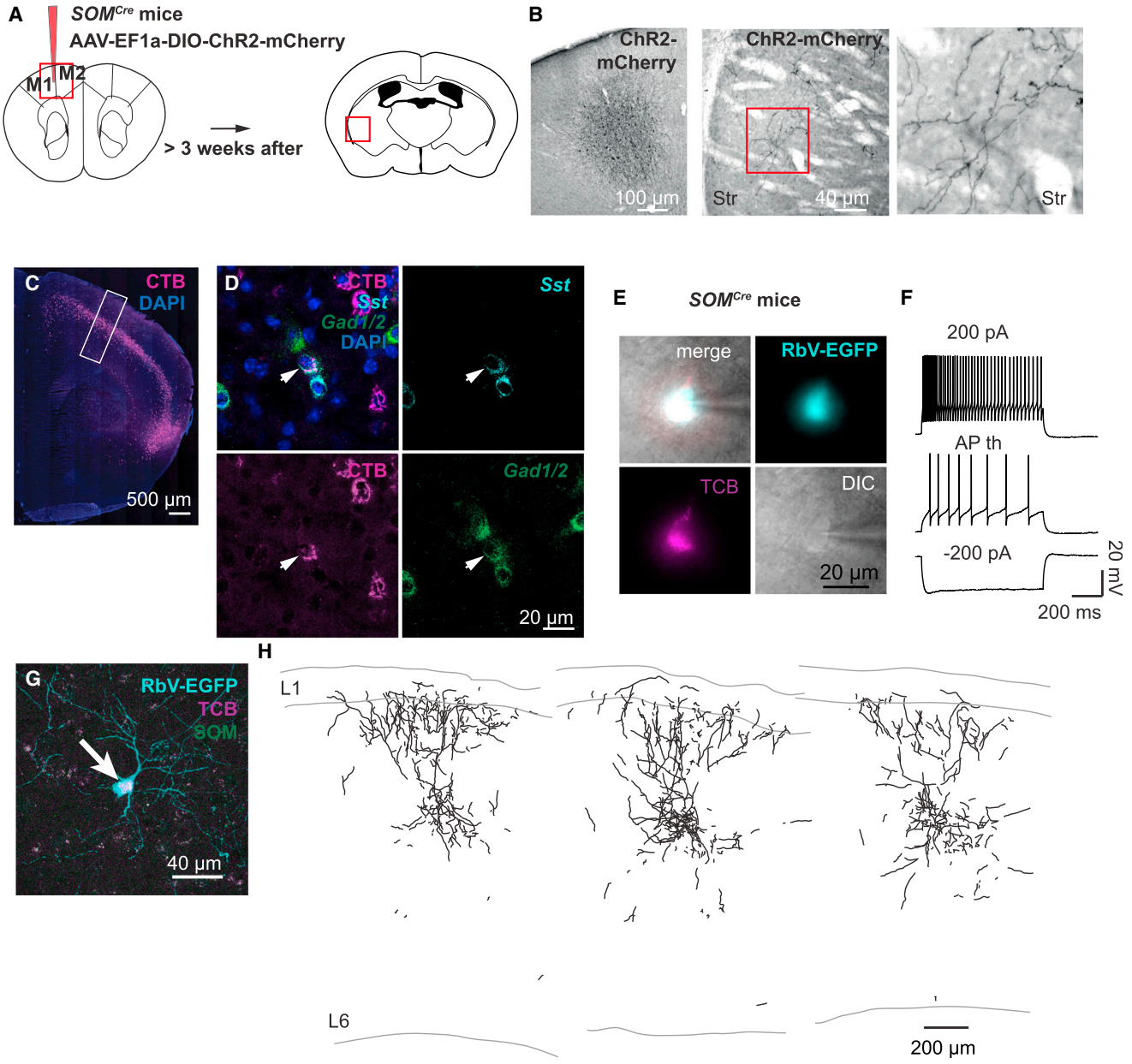

Figure 1. Motor Cortex SOM$^+$ GABAergic Neurons Innervate the Striatum

(A) Schematic drawing of the injection site and the location of long-range projections in the striatum shown in (B). Viral constructs encoding ChR2-mCherry were injected into the motor cortex of *SOM^{Cre}* mice.

(B) Bright-field images of DAB-stained sections showing the injection site in the motor cortex (left) and mCherry-labeled axons in the striatum (center) following AAV DIO *ChR2-mCherry* injection into the motor cortex of *SOM^{Cre}* mice. A higher magnification of the boxed area is shown on the right.

(C and D) Confocal images showing a retrogradely labeled area (C) following injection of the retrograde tracer CTB647 into the striatum and a retrogradely labeled GABAergic SOM$^+$ neuron in the motor cortex, visualized via FISH for *Sst* and *Gad1/2* (D).

(E–H) SOM$^+$ projecting neurons were identified by retrograde tracing with SADΔG-EGFP(EnvA) rabies virus. TCB was expressed Cre-dependently in the motor cortex of *SOM^{Cre}* mice, and rabies virus was injected into the striatum. (E) shows differential interference contrast (DIC) and epifluorescent images of a retrogradely labeled TCB$^+$ neuron in the motor cortex with the corresponding firing pattern shown in (F). (G) shows a confocal image of a retrogradely labeled TCB$^+$ neuron in M1 immunostained for EGFP and SOM with the corresponding morphological reconstruction shown in (H).

Str, striatum. See also Figure S1 and Tables S1 and S2.

et al., 2016). To substantiate and extend these studies focusing on long-range GABAergic neurons connecting the motor cortex and the striatum, we injected adeno-associated virus (AAV) double-floxed inverse open reading frame (DIO) *ChR2-mCherry* into the M1 and M2 area of *SOM^{Cre}* mice. This resulted in labeling of a subpopulation of GABAergic neurons (Figures 1A and 1B;

Figure S1A) and revealed projections in several ipsilateral cortical and subcortical areas and, to a lesser extent, in contralateral cortices (Table S1). There was consistent innervation of the ipsilateral dorsal striatum (Figure 1B; Table S1). Motor cortex SOM^+ neuron projections traversed the dorsal striatum and branched preferentially ventro-laterally, sparing the most rostral and caudal part of the dorsal striatum (Figure 1B).

To further substantiate the presence of GABAergic corticostriatal projections, we performed retrograde labeling. We injected cholera toxin B (CTB) subunit 647 into the ventro-lateral part of the dorsal striatum and analyzed retrogradely labeled cells in the M1 region (Figures S1B and S1C). As expected, a dense band of retrogradely labeled cells became visible in cortical L5 (Figure 1C); i.e., in the layer that is the major source of corticostriatal excitatory projections (Wilson, 1987; Cowan and Wilson, 1994). To visualize GABAergic cells among the M1 retrogradely labeled cells, we performed multi-fluorescence in situ hybridization (FISH) for *Sst* (encoding SOM) and *Gad1/2* (encoding GAD67/65). We found 13 retrogradely labeled cells in M1 that were clearly positive for *Gad1/2* (n = 3,582 CTB^+ cells and 5,064 $Gad1/2^+$ cells, cell counts across all layers in 35 slices from 4 hemispheres in 4 mice), 8 of which co-labeled for *Sst* (Figure 1D). Most retrogradely labeled GABAergic neurons were located in L5 (Figure S1D). To confirm a direct long-range GABAergic connection between the motor cortex (M1/M2) and the dorsal striatum, we performed retrograde monosynaptic tracing with rabies virus (Wickersham et al., 2007). We injected AAVs encoding Cre-dependent avian virus receptor (avian tumor virus receptor A mCherry [TCB]; Weissbourd et al., 2014) and rabies glycoprotein (RG) into the striatum of A2A-Cre mice that express Cre recombinase specifically in iSPNs (Gong et al., 2003). Subsequent injection of RG-deleted envelope protein from avian ASLV type A (EnvA)-pseudotyped rabies virus (SADΔG-EGFP(EnvA)) into the striatum resulted in transsynaptically retrogradely labeled cells in the cortex (Figures S1E and S1F). FISH for rabies virus-specific mRNA (*RabV-gp1*) and *Gad1/2* revealed double-positive neurons in the motor cortex (7 cells in 34 slices from 4 hemispheres in 4 mice; Figure S1G). The average number of labeled cells per slice was lower than after CTB647 injections, suggesting that iSPNs were not the only striatal target cells of GABAergic projecting neurons and/or reflecting lower efficiency of transsynaptic tracing (Marshel et al., 2010).

To determine the electrophysiological and morphological properties of SOM^+ projecting neurons, we expressed TCB Cre-dependently in the motor cortex (M1/M2) of SOM^{Cre} mice and injected SADΔG-EGFP(EnvA) rabies virus into the striatum. TCB^+ retrogradely labeled cells in the motor cortex had a classical or burst accommodating firing pattern (n = 11 cells from 5 hemispheres in 4 mice; Figures 1E and 1F; Figure S1H) similar to non-retrogradely labeled TCB^+ cells (Table S2). Reconstructed cells had a Martinotti cell-like morphology (Wang et al., 2004) with axonal projections extending over all cortical layers (three reconstructions from three hemispheres in two mice; Figures 1G and 1H; Figures S1I–S1K).

Motor Cortex Long-Range Projecting SOM^+ Neurons Differentially Inhibit Striatal Neurons

We next tested whether SOM^+ projecting neurons form functional synapses onto striatal neurons and whether the connectivity exhibits target specificity. We injected AAV DIO *ChR2-mCherry* into M1/M2 of SOM^{Cre} mice and combined optogenetic stimulation of long-range projections with patch-clamp recordings of putative postsynaptic cells in the striatum (Figure 2A). All injections (n = 36 hemispheres) resulted in labeled axons that projected to the dorsal striatum. Patched neurons were selected to be in close proximity to labeled axons. Of 305 patched neurons (in 27 mice), 50 responded with short-latency postsynaptic currents (PSCs) to 5-ms photostimulation of motor cortex SOM^+ neuron projections (Figure 2B). As a specificity control, we repeated the experiment in wild-type mice injected with AAV DIO *ChR2-mCherry* and found neither $mCherry^+$ fibers in the dorsal striatum nor a response after photostimulation (n = 58 cells in 2 mice). Responses in SOM^{Cre} mice could not be blocked with 6-cyano-2,3-dihydroxy-7-nitro-quinoxaline (CNQX) and D-2-Amino-5-Phosphonovaleric acid (D-AP5) (165.6 ± 32.7 pA baseline versus 169.5 ± 31.1 pA with drugs [mean ± SEM], paired t test, $t_{(14)} = 0.49$, p = 1, n = 15 cells in 11 mice; Figure S2A) but with gabazine (117.8 [134.3] pA versus 1.6 [1.6] pA [median interquartile range (IQR)], Wilcoxon signed-rank test, W = 210, p = 0.0002, n = 20 cells in 15 mice; Figures S2A and S2B). Responses reversed around the reversal potential of GABAergic receptors (n = 14 cells in 9 mice; Figure 2B), thus confirming the GABAergic nature of motor cortex SOM^+ neuron projections.

To scrutinize target specificity, striatal neurons were sorted into SPNs and cholinergic and GABAergic interneurons based on their electrophysiological properties and cell soma shape (Planert et al., 2013; Gertler et al., 2008; Kawaguchi, 1992; Bennett and Wilson, 1999; Kawaguchi et al., 1995; Experimental Procedures; Figures 2C–2E; Table S3). We found that 22.6% of SPNs, 33.3% of cholinergic cells, and only 2% of GABAergic interneurons responded to 5-ms photostimulation of motor cortex SOM^+ neuron projections (Figure 2F; Figures S2C and S2D; Table S3). Together, these data indicate that SPNs and cholinergic cells are the main target of motor cortex SOM^+ neuron projections.

To answer whether dSPNs and iSPNs are differentially targeted by motor cortex SOM^+ projecting neurons, we crossbred SOM^{Cre} mice to DRD1a-EGFP and DRD2-EGFP mice in which dSPNs and iSPNs, respectively, are selectively labeled (Gong et al., 2003; Figures 2G and 2H). Furthermore, we tested for differential innervation from M1 and M2. We injected AAV DIO *ChR2-mCherry* into M1 or M2 of SOM^{Cre}/DRD1a-EGFP or SOM^{Cre}/DRD2-EGFP mice (Figure 2G; Figure S2E) and combined photostimulation of M1 or M2 SOM^+ neuron projections with patch-clamp recordings of striatal neurons (Figure S2F). We found that M1 SOM^+ projecting neurons innervated a comparable proportion of dSPNs (29%), iSPNs (22%), and cholinergic cells (40%) (Figures 2I and 2J; Fisher's exact test, p = 0.19). M2 SOM^+ projecting neurons targeted dSPNs (25%) and iSPNs (16%) to a similar extent, whereas cholinergic cells tended to be innervated less frequently (4%) (Figure 2J; Fisher's exact test, p = 0.08). Inhibition of cholinergic cells by M2 was significantly less frequent than by M1 (Figure 2J; Fisher's exact test, M1 dSPNs versus M2 dSPNs: p = 1; M1 iSPNs versus M2 iSPNs: p = 1; M1 cholinergic versus M2 cholinergic: p = 0.006). Responses had a latency of 2.5 (1.3) ms (median [IQR]; n = 47

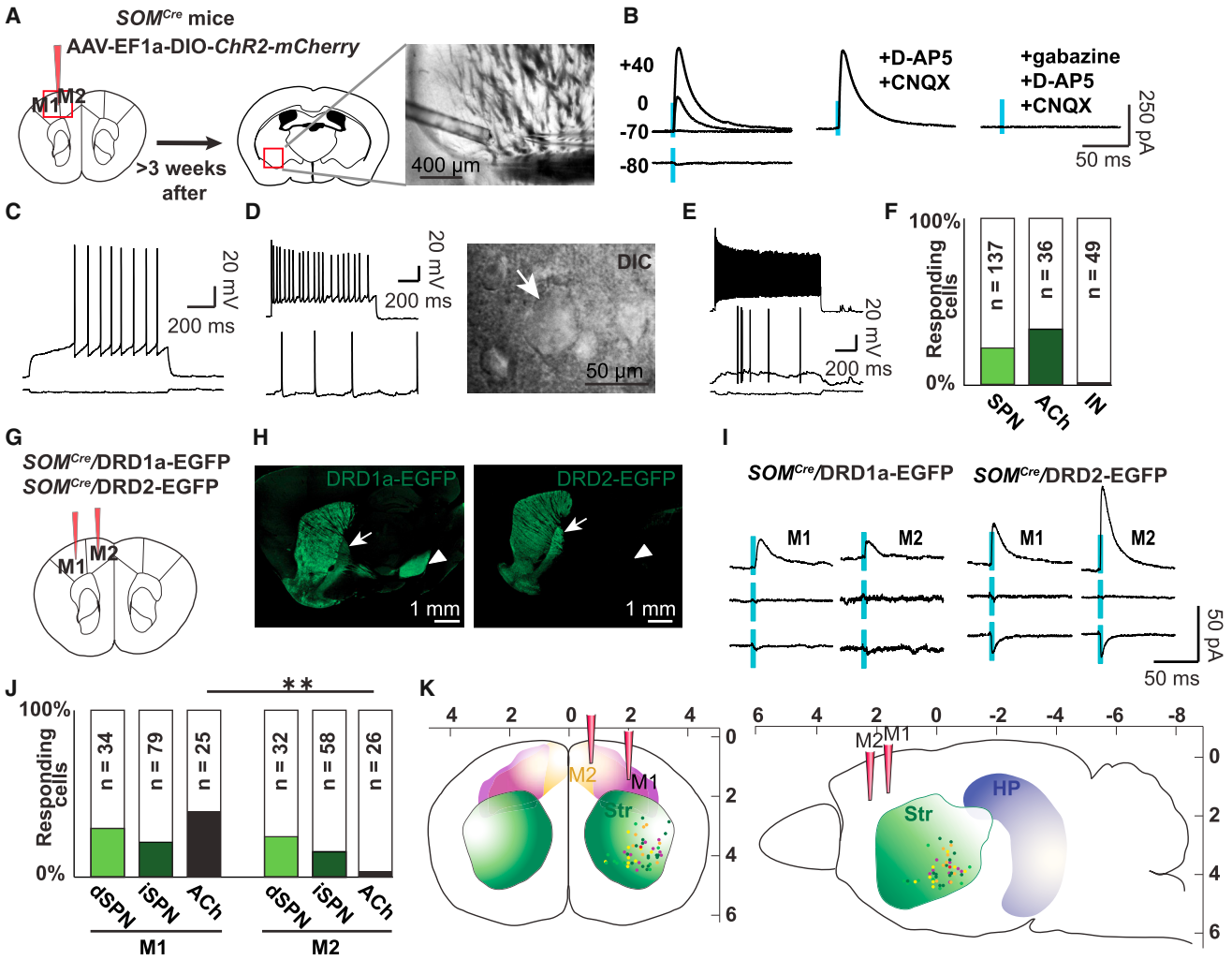

Figure 2. Motor Cortex SOM$^+$ Neuron Projections Form Functional Synapses on Striatal Output and Cholinergic Neurons

(A) Schematic drawing indicating the injection site (left) and location of an exemplary patched neuron in the striatum (right). AAV DIO *ChR2-mCherry* was injected into the motor cortex of *SOM^{Cre}* mice, and target cells were patched in the striatum (DIC image).

(B) PSCs recorded in a striatal neuron at the indicated holding potentials following 5-ms photostimulation (blue ticks) of motor cortex SOM$^+$ neuron projections. Responses were blocked with gabazine but not D-AP5/CNQX.

(C) Firing pattern (membrane potential upon −50-pA current injection and at the action potential [AP] threshold) of a representative SPN that was responsive to photostimulation of motor cortex SOM$^+$ neuron projections.

(D) Firing pattern (spontaneous activity and maximal firing frequency) and DIC image of a representative cholinergic interneuron (arrow) that was responsive to photostimulation of motor cortex SOM$^+$ neuron projections.

(E) Firing pattern of a striatal GABAergic interneuron that was responsive to photostimulation of motor cortex SOM$^+$ neuron projections (from top to bottom: maximal firing frequency, AP threshold, and −50-pA current injection).

(F) Percentage of striatal neurons responding to photostimulation of motor cortex SOM$^+$ neuron projections. The numbers in the bars indicate the total number of patched cells. Number of mice: SPNs, 19; cholinergic, 11; GABAergic interneurons, 19.

(G) Schematic drawing indicating injection sites of AAV DIO *ChR2-mCherry* in *SOM^{Cre}*/DRD1a-EGFP and *SOM^{Cre}*/DRD2-EGFP mice.

(H) Confocal image of EGFP-immunostained sagittal sections of *SOM^{Cre}*/DRD1a-EGFP (left) and *SOM^{Cre}*/DRD2-EGFP (right) mice exhibiting differential EGFP expression in the globus pallidus (arrow) and substantia nigra (arrowhead).

(I) Exemplary traces of dSPN and iSPN responses to photostimulation (blue ticks) of M1 and M2 SOM$^+$ neuron projections using Cs^+-based low Cl^- intracellular solution (from top to bottom: 0 mV, reversal potential, and −95 mV holding potential).

(J) Percentage of striatal neurons responding to photostimulation of M1 and M2 SOM$^+$ neuron projections. The numbers in the bars indicate the total number of patched cells. Number of mice: M1-dSPNs, 7; M1-iSPNs, 16; M2-dSPNs, 8; M2-iSPNs, 17; M1-cholinergic, 19; M2-cholinergic, 13.

(K) Schematic drawing indicating the localization of responding cells in a coronal (left) and sagittal (right) cross-section. Color code: orange, M1 to dSPN; yellow, M2 to dSPN; dark green, M1 to iSPN; light green, M2 to iSPN; purple, M1 to cholinergic interneuron; red, M2 to cholinergic interneuron.

HP, hippocampus; ACh, cholinergic interneuron. See also Figures S2 and S3 and Tables S3 and S4.

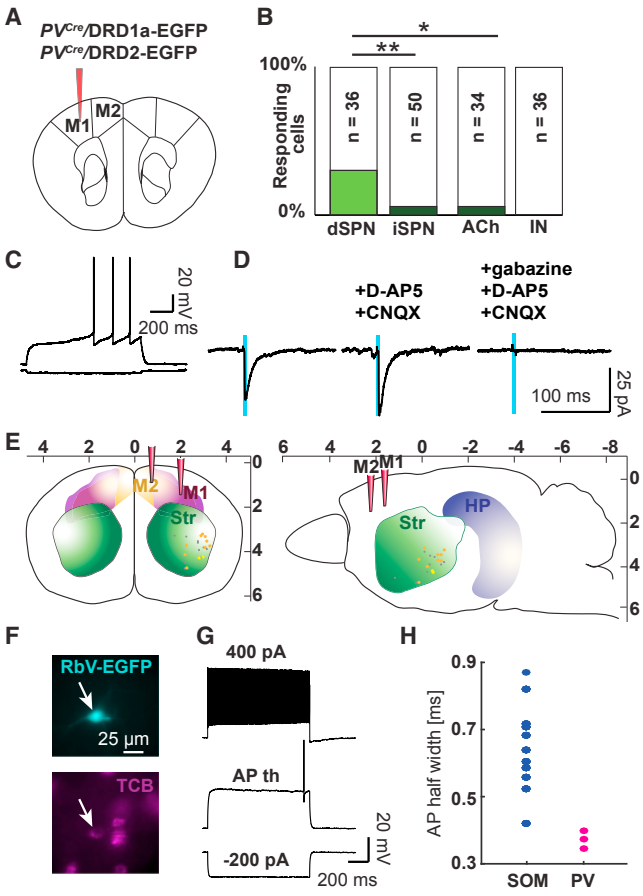

Figure 3. M1 PV$^+$ Neuron Projections Preferentially Target dSPNs in the Striatum

(A) Schematic drawing indicating the injection site of AAV DIO *ChR2-mCherry* in *PV^{Cre}*/DRD1a-EGFP and *PV^{Cre}*/DRD2-EGFP mice.

(B) Percentage of striatal neurons responding to photostimulation of M1 PV$^+$ neuron projections. The numbers indicate the total numbers of patched cells. Number of mice: dSPNs, 8; iSPNs, 7; cholinergic, 13; GABAergic interneurons, 9.

(C) Firing pattern (upon −50 pA current injection and at the AP threshold) of a representative dSPN that was responsive to photostimulation of M1 PV$^+$ neuron projections.

(D) Responses of the dSPN shown in (C) at −70 mV holding potential using high Cl$^-$ intracellular solution. Responses were blocked with gabazine but not D-AP5/CNQX.

(E) Schematic drawing indicating the localization of responding cells in a coronal (left) and sagittal (right) cross-section. Color code: orange, M1 to dSPN; yellow, M1 to iSPNs; gray, unidentified responding neurons.

(F and G) Epifluorescent images of a retrogradely labeled TCB$^+$ neuron in the motor cortex (arrow) (F) with the corresponding firing pattern (G) identified by retrograde tracing with SADΔG-EGFP(EnvA) rabies virus. TCB was expressed Cre-dependently in the motor cortex of *PV^{Cre}* mice, and rabies virus was injected into the striatum.

(H) Dot plot of the action potential half-width for retrogradely labeled SOM$^+$ (n = 11 cells from 5 hemispheres in 4 mice) and PV$^+$ neurons (n = 3 cells from 3 hemispheres in 2 mice).

See also Figure S3 and Tables S2 and S4.

responding cells; see Figure S3A and Table S4 for more details) and a reversal potential of −58.0 ± 1.4 mV (mean ± SEM; n = 22 responding cells; see Figure S3B and Table S4 for more details).

The strength of M1 and M2 SOM$^+$ neuron connections to SPNs was similar (Table S4). However, when comparing inputs with dSPNs and iSPNs both from M1 and M2, the response amplitudes were significantly larger for iSPNs (amplitudes at 0 mV with cesium [Cs$^+$] internal solution: 15.7 [29] pA versus 44.0 [36.5] pA [median (IQR)] in dSPNs and iSPNs respectively; Mann-Whitney *U* test, U = 102, p = 0.02, n = 14 and 26 responding cells, respectively; Figure S3C). Detected target cells were located preferentially in the ventro-lateral part of the dorsal striatum (Figure 2K; Figures S3D–S3F; Table S4). Targeted dSPNs and iSPNs were intermingled and localized 2.4 (0.7) mm lateral, 0.1 (0.7) mm posterior to the bregma and 4 (0.7) mm deep (median [IQR]). SPNs targeted by M1 projections were more lateral than SPNs targeted by M2 projections (Mann-Whitney *U* test, U = 142, p = 0.04; Table S4).

Motor Cortex Long-Range Projecting PV$^+$ Neurons Differentially Inhibit Striatal Neurons

The retrograde labeling experiments suggested that SOM$^+$ neurons are not the only M1 GABAergic population projecting to the striatum. PV$^+$ neurons appeared to be attractive candidates because we identified them before as a major class of neurons providing long-range inhibition in the entorhinal cortex-hippocampal formation (Melzer et al., 2012). Testing for the presence of GABAergic long-range projecting PV$^+$ cells based on virus tracing in *PV^{Cre}* mice may be complicated by the fact that a fraction of cortical PV$^+$ cells are glutamatergic (Jinno and Kosaka, 2004). Hence, we first tested the GABAergic nature of PV$^+$ cells in M1/M2 by counting the number of double-positive cells in injected *PV^{Cre}*/*GAD67^{EGFP}* mice. 99.5% of PV$^+$ cells were GAD67$^+$ (759 of 763 PV$^+$ cells from 9 slices in 3 mice). This result is in agreement with previous evidence showing the absence of PV$^+$ glutamatergic neurons in the motor cortex (Jinno and Kosaka, 2004). In the mouse neocortex, PV$^+$ and SOM$^+$ neurons constitute two non-overlapping neuronal entities (Xu et al., 2010; Tasic et al., 2016). Thus, we injected AAV DIO *ChR2-mCherry* into M1 of *PV^{Cre}* mice, and, indeed, we detected labeled axons in the dorsal striatum that branched preferentially ventro-laterally (in 12 of 17 injected hemispheres). In contrast, injections into M2 of *PV^{Cre}* mice were less likely to result in labeled striatal projections (5 of 12 injections), and projections—when present—were sparser than the ones detected after M1 injections. Thus, for a more detailed analysis of innervation patterns, we focused on projections from M1. We injected AAV DIO *ChR2-mCherry* into M1 of *PV^{Cre}*/DRD1a-EGFP or *PV^{Cre}*/DRD2-EGFP mice (Figure 3A) and found that 31% of dSPNs, 6% of iSPNs, and 6% of cholinergic and 0% of GABAergic interneurons responded to photostimulation of M1 PV$^+$ neuron projections (Figures 3B and 3C). Thus, PV$^+$ projecting neurons preferentially innervated dSPNs (Fisher's exact test; dSPNs versus iSPNs: p = 0.009, dSPNs versus cholinergic: p = 0.04, iSPNs versus cholinergic: p = 1; Figure 3B). SPNs targeted by M1 PV$^+$ projecting neurons had a response amplitude comparable with that following stimulation of M1 SOM$^+$ projections (Figure S3C; Table S4). We verified the GABAergic nature of PV$^+$ projections to the dorsal striatum pharmacologically. Although responses could not be blocked by CNQX/D-AP5 (although one of five cells showed a clear decrease in amplitude), subsequent application

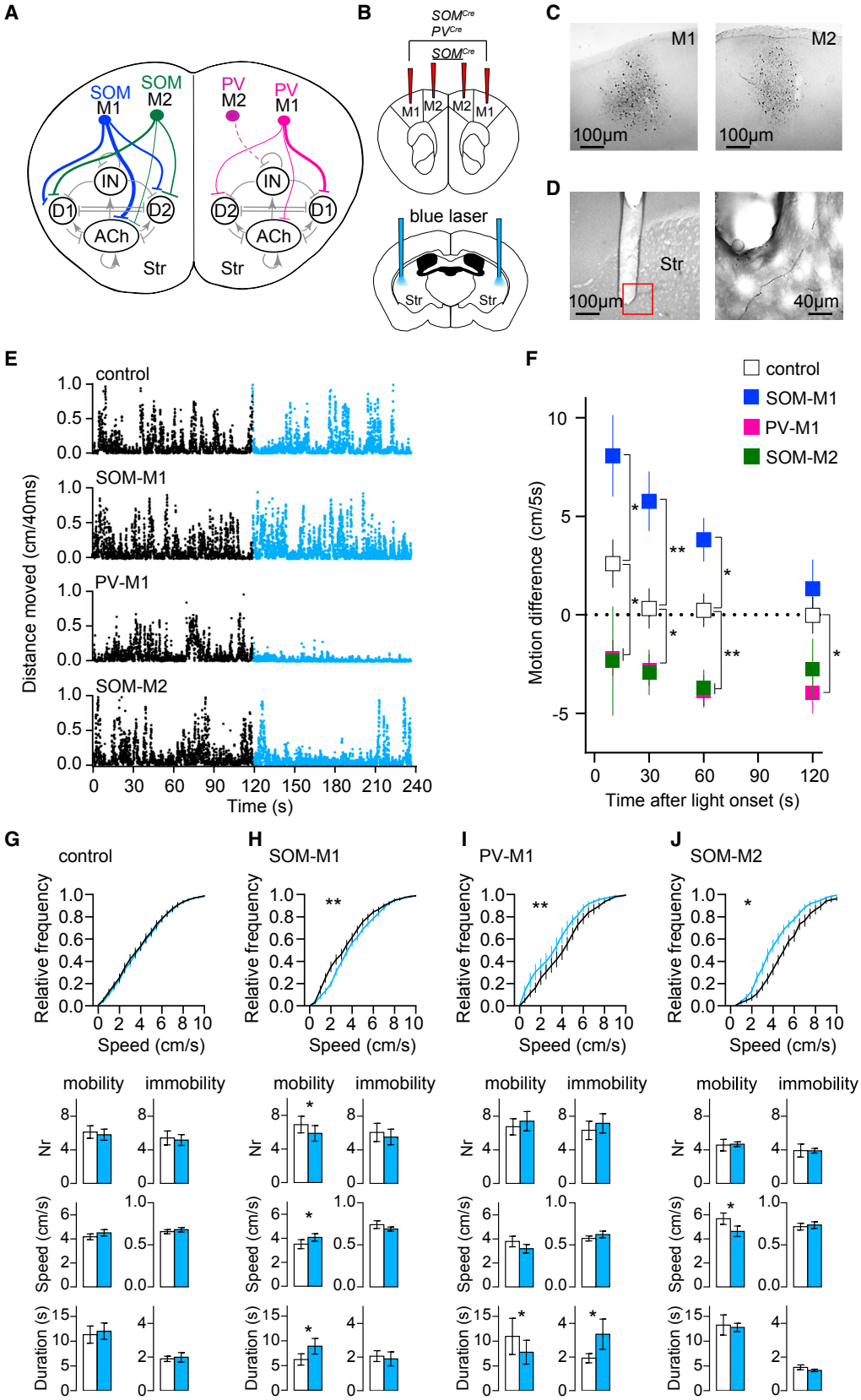

(legend on next page)

of gabazine led to a significant amplitude decrease (68.9 [147.3] pA baseline versus 70.3 [86.1] pA with CNQX/D-AP5 versus 0.5 [3.2] pA with gabazine, Friedman test, p = 0.02, post hoc Conover's test with Bonferroni correction, baseline versus CNQX/D-AP5: p = 1, baseline versus gabazine: p = 0.004, CNQX/D-AP5 versus gabazine: p = 0.009, n = 5 cells in 4 mice; Figure 3D; Figures S3G and S3H). The reversal potential of the responses was −60.3 ± 2.5 mV (mean ± SEM, n = 4 cells in 4 mice; Figure S3B; Table S4), reconfirming the GABAergic nature. SPNs targeted by M1 PV^+ projecting neurons were located 0.6 (0.7) mm posterior to the bregma, 3.0 (0.6) mm lateral, and 3.7 (0.8) deep (median [IQR]) (Figure 3E; Figures S3D–S3F; Table S4).

The different innervation patterns of SOM^+ and PV^+ projecting neurons suggested that the two cell types represent distinct subpopulations in the motor cortex. We hence analyzed whether the firing pattern of PV projecting neurons differed from that of SOM^+ projecting neurons and resembled that of "classical" PV^+ interneurons. The detection of projecting neurons was assisted by retrograde tracing with SADΔG-EGFP(EnvA) rabies virus injections into the striatum of PV^{Cre} mice expressing Cre-dependent TCB in motor cortex neurons. Indeed, all TCB^+/RbV-$EGFP^+$ non-pyramidal neurons in the motor cortex exhibited a fast spiking firing pattern with faster action potentials than SOM^+ projecting neurons (Figures 3F–3H; Figure S3I; Table S2).

Motor Cortex Long-Range Projecting SOM^+ and PV^+ Neurons Modulate Locomotor Activity

To investigate the behavioral effect of activating the newly discovered motor cortex SOM^+ and PV^+ projecting neurons (striatal targeting is summarized in Figure 4A), we implanted optic fibers bilaterally into the dorsal striatum of PV^{Cre} and SOM^{Cre} mice that were injected with AAV DIO *ChR2-mCherry* into the motor cortex (Figures 4B–4D). We compared the performance of four groups of animals: PV^{Cre} mice injected in M1 (PV-M1), SOM^{Cre} mice injected in M1 (SOM-M1), SOM^{Cre} mice injected in M2 (SOM-M2), and control mice (PV^{Cre} and SOM^{Cre} mice injected in M1 or M2 with AAV DIO *eYFP* and wild-type mice injected in M1 or M2 with AAV *Tomato*). We first asked whether activation of motor cortex PV^+ and SOM^+ neuron projections in the striatum modulated spontaneous locomotion. Mice were allowed to explore a circular arena, and locomotion was measured before and during light stimulation of corticostriatal projections (5-ms pulses at 20 Hz; power, 3 mW). We next calculated the difference between motion (defined as the distance moved in 5 s) during and before light stimulation on four epochs of different durations; i.e., 10, 30, 60, and 120 s, starting at light stimulation onset. The performance of control mice was similar before and during light stimulation (Figures 4E–4G) (the slight increase observed during the 10-s epoch was not significantly different from zero; one-sample t test (null hypothesis [H_0] = 0), $t_{(12)} = 2.1$, p = 0.06). Conversely, the performance of SOM-M1, PV-M1, and SOM-M2 changed upon photostimulation (Figures 4E and 4F). During the 10-, 30-, and 60-s epochs, SOM-M1 mice showed a significant motion increase, whereas PV-M1 and SOM-M2 mice showed a significant motion decrease with respect to control mice (Figures 4E and 4F; one-way ANOVA followed by post hoc comparisons, 10 s: $F_{(3, 31)} = 7.71$, p = 0.0005, control versus PV-M1: p = 0.03, control versus SOM-M1: p = 0.02, control versus SOM-M2: p = 0.04; 30 s: $F_{(3, 31)} = 10.48$, p = 0.0001, control versus PV-M1: p = 0.04, control versus SOM-M1: p = 0.002, control versus SOM-M2: p = 0.05; 60 s: $F_{(3, 31)} = 12.52$, p = 0.0001, control versus PV-M1: p = 0.002, control versus SOM-M1: p = 0.01, control versus SOM-M2: p = 0.008). For the 120-s epoch, only PV-M1 mice still showed a motion decrease with respect to control mice, whereas SOM-M1 and SOM-M2 performance could not be distinguished from that of control mice (Figures 4E and 4F; one-way ANOVA followed by post hoc comparisons, $F_{(3, 31)} = 3.96$, p = 0.01, control versus PV-M1: p = 0.01, control versus SOM-M1: p = 0.42, control versus SOM-M2: p = 0.13).

We characterized the photostimulation-induced motion changes occurring during the 60-s epoch in more detail. We first analyzed the cumulative frequency distribution of running speed 60 s before and for 60 s during photostimulation (Figures 4G–4J). As expected, in control mice, no difference was found between the cumulative distribution curves before and during photostimulation (Figure 4G, top; Wilcoxon matched-pairs signed-rank test, W = 193, p = 0.15). In SOM-M1 mice, the curve during photostimulation was shifted to the right, and, accordingly, the median running speed increased significantly upon photostimulation (Figure 4H, top; Wilcoxon matched-pairs signed-rank test, W = 215, p = 0.01). In PV-M1 and SOM-M2 mice, the cumulative distribution curve during photostimulation was shifted to the left, and the median running speed was significantly lower during than before photostimulation (Figures 4I and 4J, top; Wilcoxon matched-pairs signed-rank test, PV-M1: W = −113, p = 0.005; SOM-M2: W = −90, p = 0.02). Finally, based on running speed, we defined mobility and immobility bouts (Experimental Procedures) and measured their number,

Figure 4. Motor Cortex SOM^+ and PV^+ Projecting Neurons Mediate Locomotion Change

(A) Schematic drawing summarizing the newly identified corticostriatal GABAergic projections. Line thickness reflects the abundance of the distinct connections. M1 SOM^+ neurons innervate dSPNs, iSPNs, and cholinergic interneurons (blue); M2 SOM^+ neurons preferentially innervate dSPNs and iSPNs (green); M1 PV^+ neurons preferentially innervate dSPNs (pink); M2 PV^+ neuron projections are scarce (purple). D1, dSPNs; D2, iSPNs; IN, GABAergic interneuron.

(B) Schematic drawing indicating sites of AAV DIO *ChR2-mCherry* injection in SOM^{Cre} and PV^{Cre} mice (top) and of optic fiber implantation in the striatum (bottom).

(C and D) Bright-field images of DAB-stained sections showing M1 and M2 injection sites (C), optic fiber position, and mCherry-labeled axons in the striatum (D).

(E) Exemplary locomotion traces (in cm/40 ms) of control, SOM-M1, PV-M1, and SOM-M2 mice before (black) and during light stimulation (blue) (5-ms pulses delivered at 20 Hz; light power, 3 mW).

(F) Mean ± SEM difference between motion levels (in cm/5 s) during and before light stimulation for 10-, 30-, 60-, and 120-s epochs, starting at light stimulation onset.

(G–J) Mean ± SEM cumulative relative frequency of running speed (top), and mean ± SEM number, speed (in cm/s), and duration (in seconds) of mobility and immobility bouts 60 s before (black lines and white bars) and during 60-s light stimulation (blue lines and bars) for control mice (G) and SOM-M1 (H), PV-M1 (I), and SOM-M2 (J) mice. Control, n = 13 mice; SOM-M1, n = 7 mice; PV-M1, n = 9 mice; SOM-M2, n = 6 mice.

speed, and duration before and during photostimulation. In control mice, the properties of mobility and immobility bouts did not change upon photostimulation (Figure 4G; paired t test, number of bouts (nr) mobility: $t_{(12)} = 0.76$, $p = 0.46$; speed mobility: $t_{(12)} = 1.33$, $p = 0.21$; nr immobility: $t_{(12)} = 0.51$, $p = 0.62$; speed immobility: $t_{(12)} = 0.64$, $p = 0.53$; Wilcoxon matched-pairs signed-rank test: duration mobility: $W = -19$, $p = 0.54$; duration immobility: $W = -6$, $p = 0.83$). In SOM-M1 mice, photostimulation elicited significant changes in mobility bouts: the number decreased, whereas the speed and duration increased (Figure 4H; paired t test: nr: $t_{(6)} = 3.17$, $p = 0.02$; speed: $t_{(6)} = 2.97$, $p = 0.02$; Wilcoxon matched-pairs signed-rank test, duration: $W = -21$, $p = 0.03$). Immobility bouts remained unaffected (Figure 4H; paired t test: nr: $t_{(6)} = 1.46$, $p = 0.19$; speed: $t_{(6)} = 0.97$, $p = 0.37$; Wilcoxon matched-pairs signed-rank test, duration: $W = 9$, $p = 0.44$). In PV-M1 mice, the duration of mobility bouts decreased significantly, and the duration of immobility bouts increased significantly upon photostimulation (Figure 4I; Wilcoxon matched-pairs signed-rank test, duration mobility: $W = 35$, $p = 0.04$, duration immobility: $W = -39$, $p = 0.02$), whereas their number and speed remained unchanged (Figure 4I; paired t test: nr mobility: $t_{(8)} = 0.97$, $p = 0.36$; speed mobility: $t_{(8)} = 1.57$, $p = 0.14$; nr immobility: $t_{(8)} = 1.62$, $p = 0.19$; speed immobility: $t_{(6)} = 0.78$, $p = 0.46$). In SOM-M2 mice, the speed of mobility bouts was significantly reduced upon photostimulation (Figure 4J; paired t test: $t_{(5)} = 3.48$, $p = 0.02$), whereas all other variables remained unchanged (paired t test: nr mobility: $t_{(5)} = 0.14$, $p = 0.89$; nr immobility: $t_{(5)} = 0.03$, $p = 0.97$; speed immobility: $t_{(5)} = 0.26$, $p = 0.8$; Wilcoxon matched-pairs signed-rank test, duration mobility: $W = 1$, $p = 0.99$; duration immobility: $W = 11$, $p = 0.31$). In sum, we conclude that stimulation of striatal long-range projections of M1 SOM^+ neurons increased locomotion by increasing the duration and speed of mobility bouts, that stimulation of striatal long-range projections of M1 PV^+ neurons reduced locomotion by increasing the duration of immobility bouts, and that stimulation of striatal long-range projections of M2 SOM^+ neurons reduced locomotion by decreasing the speed of mobility bouts.

It has been proposed that movement control and reinforcement coding are mediated by common corticostriatal circuits (Kravitz and Kreitzer, 2012). Thus, we next asked whether stimulation of motor cortex PV^+ and SOM^+ neuron projections in the striatum also affect reinforcement/punishment coding. We tested the mice in a place preference task (Figure S4). The task lasted 3 days, during which we recorded the time mice spent in each compartment. During the first and second days (habituation and baseline, respectively), place preference was measured without photostimulation. During the third day (test), one of the compartments (stimulation side) was paired with photostimulation (5-ms pulses at 20 Hz; power, 3 mW), and place preference was measured. We calculated a difference score as the percentage of time spent on the "stimulation" side during baseline minus the percentage of time spent on the same side during the test. We found that the difference score obtained for PV-M1, SOM-M1, and SOM-M2 mice was similar to that of control mice (Figure S4B; one-way ANOVA: $F_{(3,21)} = 0.67$, $p = 0.58$). Hence, stimulation of striatal long-range projections of motor cortex PV^+ and SOM^+ neurons did not elicit place preference by employing this paradigm.

DISCUSSION

Here we show that distinct long-range GABAergic neurons connect M1 and M2 with the dorsal striatum. The newly identified long-range GABAergic neurons express either SOM or PV and differ with respect to target cell preference and the modulatory effect on motor activity.

Our results indicate that both M1 and M2 harbor long-range GABAergic neurons that target the dorsal striatum and thus extend recent findings by Rock et al. (2016). Furthermore, we report the following new findings. First, M1 and M2 contribute differentially to GABAergic corticostriatal projections. Second, we identified and characterized an additional projection formed by PV^+ neurons that differs significantly from that formed by SOM^+ neurons. And third, we demonstrate that these corticostriatal GABAergic projections modulate behavior. Multiple reasons can explain why these connections have not been noticed until recently (Rock et al., 2016). First, the scarcity of long-range GABAergic neurons constitutes a challenge as to their detection by anterograde or retrograde labeling, considering the high number of excitatory neurons that are also labeled in the same area with their axons extending along a similar path. Second, most studies focused on more dorso-anterior areas of the striatum. Hence, retrograde tracer injections are unlikely to reveal GABAergic projecting neurons in motor cortices because their axons target preferentially more lateral, posterior, and ventral parts of the dorsal striatum. However, Jinno and Kosaka (2004) did not detect motor cortical long-range GABAergic neurons even though injections included target areas that were innervated in our study. A possible reason may be low uptake efficiency and transport of the tracer FluoroGold in GABAergic neurons.

We confirmed the existence of GABAergic corticostriatal projections employing several approaches. First, there was robust axon labeling in the striatum even with regionally restricted minimal anterograde injections. Second, long-range GABAergic neurons were retrogradely labeled with CTB from the striatum. Third, long-range GABAergic neurons were transsynaptically retrogradely labeled with rabies virus that infected only striatal starter cells. Finally, the electrophysiological and pharmacological results provide strong evidence for the GABAergic nature of PV^+ and SOM^+ projecting neurons. Although we have no indication for any glutamatergic inputs deriving from SOM^+ cells, based on our immunocytochemistry, pharmacology, and rabies virus tracing, we cannot exclude that glutamatergic transmission has a minor contribution to the behavioral effects seen upon stimulation of striatal long-range projections from M1 PV^+ neurons.

It is important to note that the number of long-range GABAergic neurons presented in this study remains an underestimation because quantitative evaluations are currently hampered by a number of technical constraints. First, experiments entail "conservative/limited" virus injection to prevent viral spread beyond the target area. Second, labeling by retrograde tracing is strongly dependent on the tracer and cell type; e.g., PV^+ neurons could be detected following transsynaptic virus-mediated tracing but not by CTB labeling. For quantitative studies, it would be highly desirable to identify markers/promoters for long-range GABAergic neurons.

Characterization of motor cortex GABAergic projecting neurons revealed that M1 and M2 SOM$^+$ and PV$^+$ cells differentially innervate striatal neurons. Moreover, bilateral stimulation of corticostriatal long-range GABAergic projections modulates motor activity in spite of the scarcity of GABAergic corticostriatal neurons and the relatively small amplitude responses of targeted striatal neurons. Thus, stimulation of M1 SOM$^+$ neuron projections, targeting dSPNs, iSPNs, and cholinergic cells, leads to an increase in locomotion. In contrast, stimulation of M2 SOM$^+$ neuron projections, targeting preferentially dSPNs and iSPNs, and of M1 PV$^+$ neuron projections, targeting preferentially dSPNs, leads to a decrease in locomotion. Decreased locomotion upon preferential inhibition of dSPNs (PV-M1) is in line with previous studies showing either bradykinesia upon deletion of dSPNs (Drago et al., 1998) or increased locomotion upon stimulation of dSPNs (Kravitz et al., 2010). Notably, there was a similar effect on locomotion upon preferential inhibition of dSPNs (PV-M1) or of both dSPNs and iSPNs (SOM-M2). Comparable effects were also reported when optogenetically silencing either dSPN or both dSPNs and iSPNs (Tecuapetla et al., 2014). Increased locomotion upon stimulation of M1 SOM$^+$ neuron projections most likely reflects the participation of a larger fraction of cholinergic cells. These striatal interneurons, constituting 1%–3% of all striatal neurons, are tonically active and provide powerful feedforward inhibition to SPNs (English et al., 2011; Nelson et al., 2014), modulate corticostriatal synapses (Calabresi et al., 1998; Higley et al., 2009), and enhance dopamine release (Threlfell et al., 2012). Direct activation or inhibition of cholinergic striatal interneurons in the dorsal anterior striatum had no effect on locomotor activity (Maurice et al., 2015). However, based on our results, it is tempting to speculate that cholinergic cells in more ventral and posterior striatal areas receiving input from M1 SOM$^+$ neurons are involved in motor control. At present, we cannot resolve whether the observed change in locomotor activity results from long-range axon activation in the striatum only or whether activation of putative collaterals via back-propagating action potentials also plays a role. In either case, our results show that the activity of SOM$^+$ and PV$^+$ projecting neurons in the motor cortex differentially modulates locomotor activity. This study is also relevant when interpreting data regarding silencing of cortical areas by manipulating GABAergic neurons because the effects may also involve long-distance targets.

It has been proposed that motor control and reward coding are mediated by common corticostriatal circuits (Kravitz and Kreitzer, 2012). Our data indicate that, although activation of motor cortex PV$^+$ and SOM$^+$ neuron projections in the dorsal striatum affected locomotor activity, it did not affect place preference, although we cannot exclude their implication in reward coding more generally. On the other hand, stimulation of GABAergic projections from the prefrontal cortex to the ventral striatum induces avoidance behavior, suggesting that they are involved in the coding of punishment (Lee et al., 2014). Locomotion modulation was not addressed in the latter study. Further experiments will be required to elucidate whether, and, if so, which, corticostriatal GABAergic projections mediate both locomotion and reward coding.

This study adds to the increasing evidence that long-range GABAergic neurons are more frequent than previously thought. The heterogeneity of long-range GABAergic neurons described here is in line with previous studies indicating neurochemical diversity of long-range GABAergic neurons in the cortex and hippocampus (Jinno et al., 2007; Higo et al., 2007; Lee et al., 2014; Tomioka et al., 2005; Tomioka and Rockland, 2007). Notably, we demonstrate that distinct long-range GABAergic neurons exhibit specific functional properties and differential connectivity.

Finally, it will be of interest to study long-range GABAergic neurons in the context of movement disorders that are thought to be caused by an imbalance of dSPN and iSPN activity. Thus, parkinsonian-like movements can be reproduced by increased iSPN activity (Kravitz et al., 2010) and can be reduced by selective inhibition of striatal cholinergic interneurons (Maurice et al., 2015). Huntington's disease is marked by an early degeneration of iSPNs (Vonsattel et al., 1985; Mitchell et al., 1999) and an imbalance of excitation and inhibition of dSPNs and iSPNs (André et al., 2011). In light of our findings, it is tempting to speculate that motor cortex GABAergic projections to the striatum might be a potential target for restoring the balance of striatal output.

EXPERIMENTAL PROCEDURES

More detailed information is available in the Supplemental Experimental Procedures.

All experiments were performed in 8- to 20-week-old male mice and were approved by the Regierungspräsidium Karlsruhe in compliance with the European Guidelines for the Care and Use of Laboratory Animals (licenses G74/13 and G248/14).

Intracranial Injections and Optic Fiber Implantation

For anterograde tracing experiments, in vitro patch-clamp recordings, and behavioral experiments, AAV DIO *ChR2-mCherry* was injected into the primary and/or secondary motor cortex of *SOM^{Cre}* (Melzer et al., 2012), *PV^{Cre}* (Hippenmeyer et al., 2005), *PV^{Cre}*/GAD67-EGFP (Tamamaki et al., 2003), *SOM^{Cre}*/DRD1a-EGFP, *PV^{Cre}*/DRD1a-EGFP, *SOM^{Cre}*/DRD2-EGFP (Gong et al., 2003), and *PV^{Cre}*/DRD2-EGFP mice with a C57BL/6 background. For retrograde tracing experiments, CTB 647 was injected into the dorsal striatum of wild-type mice. For retrograde transsynaptic rabies virus tracing, AAV-CAG-Flex-TCB, AAV-CAG-Flex-RG, and SADΔG-EGFP(EnvA) were injected into the dorsal striatum of A2A-Cre mice. For monosynaptic retrograde rabies virus tracing, AAV-CAG-Flex-TCB was injected into the motor cortex of *SOM^{Cre}* (*Sst$^{tm2.1(cre)Zjh}$*, Jackson Laboratory) and *PV^{Cre}* mice, followed by SADΔG-EGFP(EnvA) injection into the dorsal striatum. In all cases, anesthesia was induced and maintained with isoflurane (1%–2.5%), and the virus was delivered through a small craniotomy at the appropriate coordinates by a glass micropipette. For behavioral experiments, optic fiber cannulas were bilaterally implanted into the striatum after viral injections.

Immunohistochemistry

Mice were transcardially perfused with 4% paraformaldehyde (PFA). Immunofluorescence and DAB staining were performed on sagittal and coronal brain sections using standard protocols.

FISH

Mice were deeply anesthetized with isoflurane and decapitated. Fresh-frozen 20-μm sections were stained with FISH using the RNAscope Fluorescent Multiplex kit (Advanced Cell Diagnostics).

In Vitro Patch-Clamp Recordings

Mice were deeply anesthetized with isoflurane, transcardially perfused with ~30 mL ice-cold sucrose solution, and 300-μm-thick brain sections were cut. ChR2-expressing long-range axonal fibers were stimulated with 5-ms

photostimulation (473 nm, 120 mW/mm^2 laser intensity). PSCs were measured at 0-mV holding potential (using Cs^+-based intracellular solution) or at −70-mV holding potential (using K^+-based, high Cl^- intracellular solution). For firing pattern analysis, incrementally increasing currents of 1-s duration were injected in current clamp mode starting at −50 or −200 pA. Series resistances of 37 megohm were accepted for analysis of PSCs. Stimulus delivery and data acquisition were performed using Pulse software. Data analysis was performed with MATLAB.

Behavioral Experiments

Mice were video-tracked at 25 frames/s, and their movements were subsequently analyzed using a position tracking system (Ethovision XT9, Noldus). The implanted optic fiber cannulas were connected to two optic fibers attached to a rotary joint (Doric Lenses). A patch cord connected the optic fibers to a diode-pumped, solid-state, 473-nm laser (CrystaLaser). We used a pulse generator (Master 8) and a transistor-transistor logic (TTL) control box (universal serial bus input/output [USB-IO] box, Noldus) to automatically control the photostimulation (5-ms pulses delivered at 20 Hz; laser power, 3 mW). Evaluation of locomotor activity was performed in a circular arena (40 × 40 cm) placed in a dimly lit room where mice were allowed to run freely for 21 min. After an initial 5-min acclimation phase, photostimulation started. It lasted 2 min and was repeated three times with an inter-stimulation period of 4 min.

Statistics

The Shapiro-Wilk test was used to test for normal distribution. Brown-Forsythe and F tests were used to test the homogeneity of variances. For non-pairwise comparisons, unpaired t tests (either for equal or unequal variance) or Mann-Whitney *U* tests were used. For pairwise comparisons, paired t tests or Wilcoxon matched-pairs signed-rank tests were used. Proportions were compared using Fisher's exact tests. For multiple pairwise comparisons, Friedman test followed by post hoc Conovor's tests was used. One-way ANOVA followed by Tukey's multiple comparisons tests was used to compare motion differences.

SUPPLEMENTAL INFORMATION

Supplemental Information includes Supplemental Experimental Procedures, four figures, and four tables and can be found with this article online at http://dx.doi.org/10.1016/j.celrep.2017.04.024.

AUTHOR CONTRIBUTIONS

S.M., M.G., and H.M. designed the experiments and wrote the manuscript with contributions from all authors. S.M. performed in vitro electrophysiology, analysis, immunohistochemistry, reconstructions, and retrograde tracing studies. M.G. performed behavioral experiments and corresponding analyses. D.E.K. performed control electrophysiological experiments and immunostaining. M.M. performed immunohistochemistry and virus injections. K.W.H. produced the pseudotyped rabies virus.

ACKNOWLEDGMENTS

We thank K. Deisseroth for the AAVs and B. L. Sabatini for providing AAVs, rabies virus, and FISH reagents; I. Preugschat-Gumprecht, U. Amtmann, R. Hinz, and B. Schwalm for technical assistance; E. Senkova for AAV injections and optic fiber implantations; and Byung Kook Lim for providing starting material for rabies virus production. The research was funded by European Research Council Grant FP 7 and ERC Advanced Grant 250047 (to H.M.) German Research Foundation (DFG) Grants MO432/10 (to H.M.), SFB1134 (to H.M.), and GI1157/1-1 (to M.G.), and German Ministry of Education and Research (BMBF) Grant 01GQ1003A (to H.M.).

Received: March 26, 2016
Revised: March 21, 2017
Accepted: April 9, 2017
Published: May 2, 2017

REFERENCES

André, V.M., Fisher, Y.E., and Levine, M.S. (2011). Altered Balance of Activity in the Striatal Direct and Indirect Pathways in Mouse Models of Huntington's Disease. Front. Syst. Neurosci. *5*, 46.

Bennett, B.D., and Wilson, C.J. (1999). Spontaneous activity of neostriatal cholinergic interneurons in vitro. J. Neurosci. *19*, 5586–5596.

Bolam, J.P., Hanley, J.J., Booth, P.A., and Bevan, M.D. (2000). Synaptic organisation of the basal ganglia. J. Anat. *196*, 527–542.

Calabresi, P., Centonze, D., Gubellini, P., Pisani, A., and Bernardi, G. (1998). Endogenous ACh enhances striatal NMDA-responses via M1-like muscarinic receptors and PKC activation. Eur. J. Neurosci. *10*, 2887–2895.

Cowan, R.L., and Wilson, C.J. (1994). Spontaneous firing patterns and axonal projections of single corticostriatal neurons in the rat medial agranular cortex. J. Neurophysiol. *71*, 17–32.

Drago, J., Padungchaichot, P., Wong, J.Y., Lawrence, A.J., McManus, J.F., Sumarsono, S.H., Natoli, A.L., Lakso, M., Wreford, N., Westphal, H., et al. (1998). Targeted expression of a toxin gene to D1 dopamine receptor neurons by cre-mediated site-specific recombination. J. Neurosci. *18*, 9845–9857.

English, D.F., Ibanez-Sandoval, O., Stark, E., Tecuapetla, F., Buzsáki, G., Deisseroth, K., Tepper, J.M., and Koos, T. (2011). GABAergic circuits mediate the reinforcement-related signals of striatal cholinergic interneurons. Nat. Neurosci. *15*, 123–130.

Fuchs, E.C., Neitz, A., Pinna, R., Melzer, S., Caputi, A., and Monyer, H. (2016). Local and distant input controlling excitation in layer II of the medial entorhinal cortex. Neuron *89*, 194–208.

Gertler, T.S., Chan, C.S., and Surmeier, D.J. (2008). Dichotomous anatomical properties of adult striatal medium spiny neurons. J. Neurosci. *28*, 10814–10824.

Gong, S., Zheng, C., Doughty, M.L., Losos, K., Didkovsky, N., Schambra, U.B., Nowak, N.J., Joyner, A., Leblanc, G., Hatten, M.E., and Heintz, N. (2003). A gene expression atlas of the central nervous system based on bacterial artificial chromosomes. Nature *425*, 917–925.

Higley, M.J., Soler-Llavina, G.J., and Sabatini, B.L. (2009). Cholinergic modulation of multivesicular release regulates striatal synaptic potency and integration. Nat. Neurosci. *12*, 1121–1128.

Higo, S., Udaka, N., and Tamamaki, N. (2007). Long-range GABAergic projection neurons in the cat neocortex. J. Comp. Neurol. *503*, 421–431.

Hippenmeyer, S., Vrieseling, E., Sigrist, M., Portmann, T., Laengle, C., Ladle, D.R., and Arber, S. (2005). A developmental switch in the response of DRG neurons to ETS transcription factor signaling. PLoS Biol. *3*, e159.

Jinno, S., and Kosaka, T. (2004). Parvalbumin is expressed in glutamatergic and GABAergic corticostriatal pathway in mice. J. Comp. Neurol. *477*, 188–201.

Jinno, S., Klausberger, T., Marton, L.F., Dalezios, Y., Roberts, J.D.B., Fuentealba, P., Bushong, E.A., Henze, D., Buzsáki, G., and Somogyi, P. (2007). Neuronal diversity in GABAergic long-range projections from the hippocampus. J. Neurosci. *27*, 8790–8804.

Kawaguchi, Y. (1992). Large aspiny cells in the matrix of the rat neostriatum in vitro: physiological identification, relation to the compartments and excitatory postsynaptic currents. J. Neurophysiol. *67*, 1669–1682.

Kawaguchi, Y., Wilson, C.J., Augood, S.J., and Emson, P.C. (1995). Striatal interneurones: chemical, physiological and morphological characterization. Trends Neurosci. *18*, 527–535.

Koralek, A.C., Jin, X., Long, J.D., 2nd, Costa, R.M., and Carmena, J.M. (2012). Corticostriatal plasticity is necessary for learning intentional neuroprosthetic skills. Nature *483*, 331–335.

Kravitz, A.V., and Kreitzer, A.C. (2012). Striatal mechanisms underlying movement, reinforcement, and punishment. Physiology (Bethesda). *27*, 167–177.

Kravitz, A.V., Freeze, B.S., Parker, P.R.L., Kay, K., Thwin, M.T., Deisseroth, K., and Kreitzer, A.C. (2010). Regulation of parkinsonian motor behaviours by optogenetic control of basal ganglia circuitry. Nature *466*, 622–626.

Kravitz, A.V., Tye, L.D., and Kreitzer, A.C. (2012). Distinct roles for direct and indirect pathway striatal neurons in reinforcement. Nat. Neurosci. *15*, 816–818.

Lee, A.T., Vogt, D., Rubenstein, J.L., and Sohal, V.S. (2014). A class of GABAergic neurons in the prefrontal cortex sends long-range projections to the nucleus accumbens and elicits acute avoidance behavior. J. Neurosci. *34*, 11519–11525.

Marshel, J.H., Mori, T., Nielsen, K.J., and Callaway, E.M. (2010). Targeting single neuronal networks for gene expression and cell labeling in vivo. Neuron *67*, 562–574.

Maurice, N., Liberge, M., Jaouen, F., Ztaou, S., Hanini, M., Camon, J., Deisseroth, K., Amalric, M., Kerkerian-Le Goff, L., and Beurrier, C. (2015). Striatal Cholinergic Interneurons Control Motor Behavior and Basal Ganglia Function in Experimental Parkinsonism. Cell Rep. *13*, 657–666.

McGeorge, A.J., and Faull, R.L. (1989). The organization of the projection from the cerebral cortex to the striatum in the rat. Neuroscience *29*, 503–537.

Melzer, S., Michael, M., Caputi, A., Eliava, M., Fuchs, E.C., Whittington, M.A., and Monyer, H. (2012). Long-range-projecting GABAergic neurons modulate inhibition in hippocampus and entorhinal cortex. Science *335*, 1506–1510.

Mitchell, I.J., Cooper, A.J., and Griffiths, M.R. (1999). The selective vulnerability of striatopallidal neurons. Prog. Neurobiol. *59*, 691–719.

Nelson, A.B., Hammack, N., Yang, C.F., Shah, N.M., Seal, R.P., and Kreitzer, A.C. (2014). Striatal cholinergic interneurons Drive GABA release from dopamine terminals. Neuron *82*, 63–70.

Planert, H., Berger, T.K., and Silberberg, G. (2013). Membrane properties of striatal direct and indirect pathway neurons in mouse and rat slices and their modulation by dopamine. PLoS ONE *8*, e57054.

Rock, C., Zurita, H., Wilson, C., and Apicella, A.J. (2016). An inhibitory corticostriatal pathway. eLife *5*, 15890.

Tamamaki, N., Yanagawa, Y., Tomioka, R., Miyazaki, J., Obata, K., and Kaneko, T. (2003). Green fluorescent protein expression and colocalization with calretinin, parvalbumin, and somatostatin in the GAD67-GFP knock-in mouse. J. Comp. Neurol. *467*, 60–79.

Tasic, B., Menon, V., Nguyen, T.N., Kim, T.K., Jarsky, T., Yao, Z., Levi, B., Gray, L.T., Sorensen, S.A., Dolbeare, T., et al. (2016). Adult mouse cortical cell taxonomy revealed by single cell transcriptomics. Nat. Neurosci. *19*, 335–346.

Tecuapetla, F., Matias, S., Dugue, G.P., Mainen, Z.F., and Costa, R.M. (2014). Balanced activity in basal ganglia projection pathways is critical for contraversive movements. Nat. Commun. *5*, 4315.

Threlfell, S., Lalic, T., Platt, N.J., Jennings, K.A., Deisseroth, K., and Cragg, S.J. (2012). Striatal dopamine release is triggered by synchronized activity in cholinergic interneurons. Neuron *75*, 58–64.

Tomioka, R., and Rockland, K.S. (2007). Long-distance corticocortical GABAergic neurons in the adult monkey white and gray matter. J. Comp. Neurol. *505*, 526–538.

Tomioka, R., Okamoto, K., Furuta, T., Fujiyama, F., Iwasato, T., Yanagawa, Y., Obata, K., Kaneko, T., and Tamamaki, N. (2005). Demonstration of long-range GABAergic connections distributed throughout the mouse neocortex. Eur. J. Neurosci. *21*, 1587–1600.

Vonsattel, J.P., Myers, R.H., Stevens, T.J., Ferrante, R.J., Bird, E.D., and Richardson, E.P., Jr. (1985). Neuropathological classification of Huntington's disease. J. Neuropathol. Exp. Neurol. *44*, 559–577.

Wang, Y., Toledo-Rodriguez, M., Gupta, A., Wu, C., Silberberg, G., Luo, J., and Markram, H. (2004). Anatomical, physiological and molecular properties of Martinotti cells in the somatosensory cortex of the juvenile rat. J. Physiol. *561*, 65–90.

Weissbourd, B., Ren, J., DeLoach, K.E., Guenthner, C.J., Miyamichi, K., and Luo, L. (2014). Presynaptic partners of dorsal raphe serotonergic and GABAergic neurons. Neuron *83*, 645–662.

Wickersham, I.R., Lyon, D.C., Barnard, R.J., Mori, T., Finke, S., Conzelmann, K.K., Young, J.A., and Callaway, E.M. (2007). Monosynaptic restriction of transsynaptic tracing from single, genetically targeted neurons. Neuron *53*, 639–647.

Wilson, C.J. (1987). Morphology and synaptic connections of crossed corticostriatal neurons in the rat. J. Comp. Neurol. *263*, 567–580.

Wu, Y., Richard, S., and Parent, A. (2000). The organization of the striatal output system: a single-cell juxtacellular labeling study in the rat. Neurosci. Res. *38*, 49–62.

Xiong, Q., Znamenskiy, P., and Zador, A.M. (2015). Selective corticostriatal plasticity during acquisition of an auditory discrimination task. Nature *521*, 348–351.

Xu, X., Roby, K.D., and Callaway, E.M. (2010). Immunochemical characterization of inhibitory mouse cortical neurons: three chemically distinct classes of inhibitory cells. J. Comp. Neurol. *518*, 389–404.

Znamenskiy, P., and Zador, A.M. (2013). Corticostriatal neurons in auditory cortex drive decisions during auditory discrimination. Nature *497*, 482–485.

Cell Reports, Volume *19*

Supplemental Information

Distinct Corticostriatal GABAergic Neurons Modulate Striatal Output Neurons and Motor Activity

Sarah Melzer, Mariana Gil, David E. Koser, Magdalena Michael, Kee Wui Huang, and Hannah Monyer

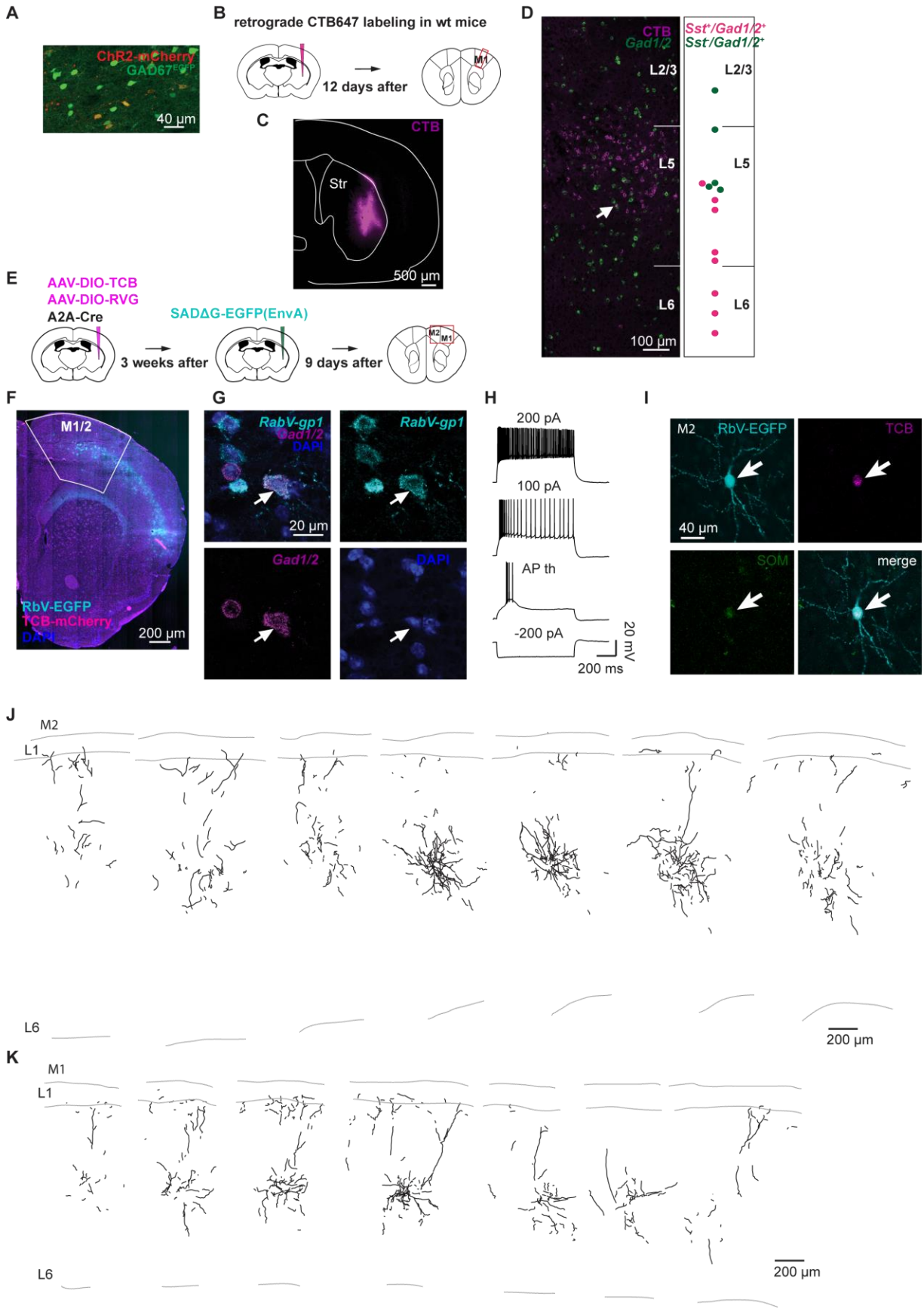
A
ChR2-mCherry
GAD67EGFP
40 µm
B
retrograde CTB647 labeling in wt mice
12 days after
M1
C
CTB
Str
500 µm
D
CTB
Gad1/2
L2/3
L5
L6
100 µm
Sst+/Gad1/2+
Sst-/Gad1/2+
E
AAV-DIO-TCB
AAV-DIO-RVG
A2A-Cre
SADΔG-EGFP(EnvA)
3 weeks after
9 days after
M2
M1
F
M1/2
RbV-EGFP
TCB-mCherry
DAPI
200 µm
G
RabV-gp1
Gad1/2
DAPI
20 µm
H
200 pA
100 pA
AP th
-200 pA
20 mV
200 ms
I
M2
RbV-EGFP
TCB
40 µm
SOM
merge
J
M2
L1
L6
200 µm
K
M1
L1
L6
200 µm

Figure S1 (related to Figure 1)

Martinotti cells in deep layers of motor cortex project to striatum

(A) Confocal image showing mCherry expression in GABAergic neurons following virus-injection into the motor cortex of a $SOM^{Cre}/GAD67^{EGFP}$ mouse.

(B) Schematic drawing indicating injection site of CTB647 in the striatum and site of analysis of retrogradely labeled neurons.

(C) Confocal image showing injection site following injection of the retrograde tracer CTB647 into striatum.

(D) Fluorescent image of cortical layers 2-6 stained with FISH indicating the localization of the retrogradely labeled GABAergic neuron shown in Figure 1D. Approximate borders of layers 2-6 are indicated. Schematic drawing on the right indicates location of all identified SOM^+ and SOM^- retrogradely labeled GABAergic cells in M1.

(E) Schematic drawing showing the protocol steps of transsynaptic labeling employing rabies viruses (SADΔG-EGFP(EnvA)) to reveal corticostriatal GABAergic neurons targeting infected iSPNs.

(F) Injection of Cre-dependent viral constructs encoding TCB-mCherry and rabies glycoprotein into the striatum of A2A-Cre mice followed by injection of SADΔG-EGFP(EnvA) rabies virus into striatum results in typical retrograde labeling (RbV-$EGFP^+$) of cortical neurons mainly in L5. Box indicates area that was screened for retrogradely labeled GABAergic neurons.

(G) Confocal images of a retrogradely labeled GABAergic neuron in motor cortex (arrow) revealed by FISH for *Gad1/2* and rabies mRNA (*RabV-gp1*) after virus injections as depicted in E.

(H) Firing pattern of a burst accommodating SOM^+ projecting neuron identified by retrograde tracing with SADΔG-EGFP(EnvA) rabies virus. TCB was expressed Cre-dependently in the motor cortex of SOM^{Cre} mice and rabies virus was injected into striatum.

(I) Confocal images of a SOM^+ projecting neuron in M2 identified based on its TCB-mCherry, RbV-EGFP and SOM expression after injection of AAV DIO *TCB-mCherry* and SADΔG-EGFP(EnvA) into motor cortex and striatum of SOM^{Cre} mice respectively.

(J) Corresponding morphological reconstruction of the projecting neuron shown in (I).

(K) Reconstructed $SOM^+/TCB^+/EGFP^+$ projecting neuron in M1.

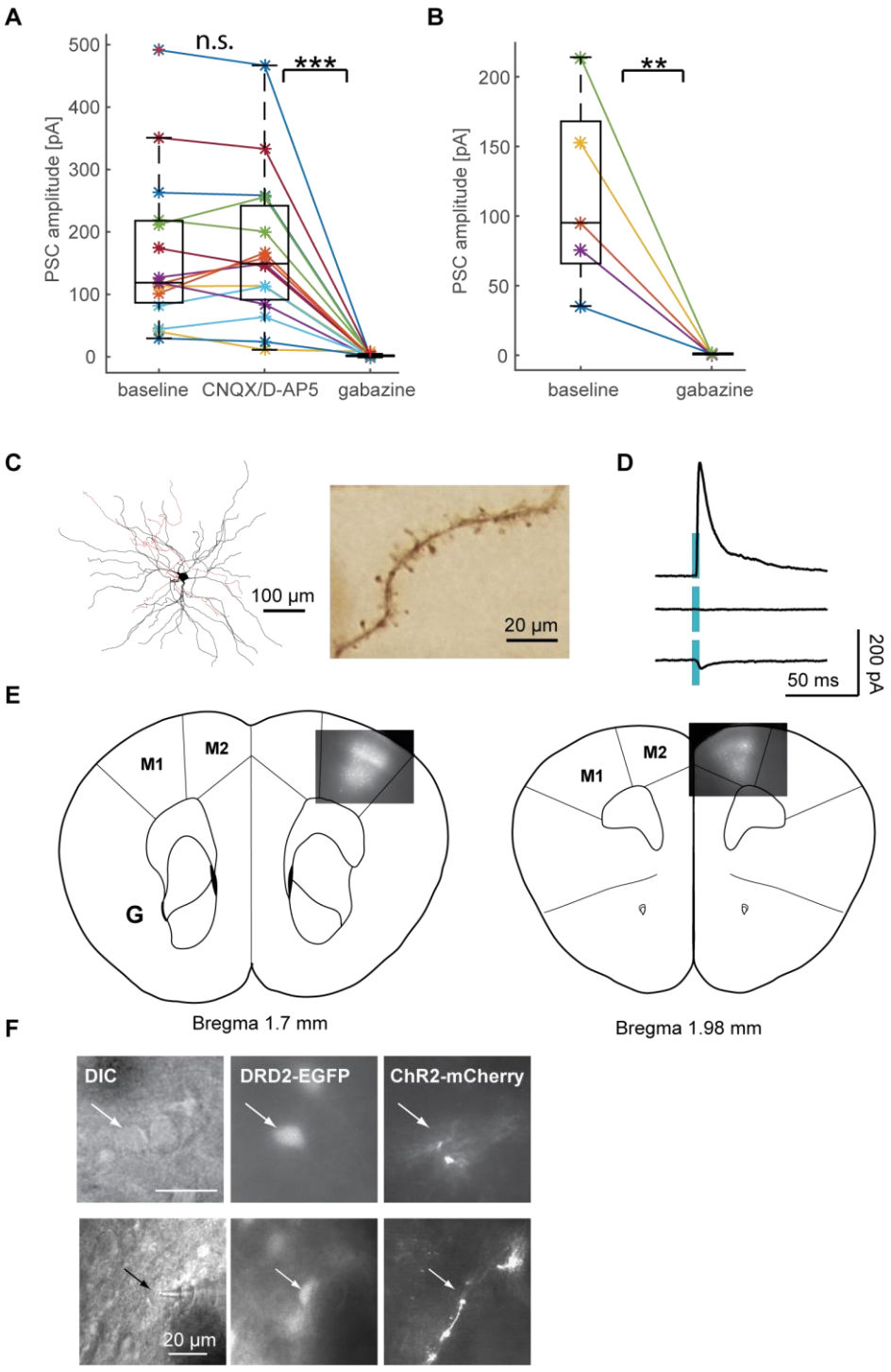

Figure S2 (related to Figure 2)

Long-range SOM$^+$ projections originating in the motor cortex target striatal output neurons and interneurons

(A-B) Dot/box plots (median (IQR), range) indicating the PSC amplitudes of striatal target neurons upon photostimulation of SOM$^+$ projecting neurons before (baseline) and after drug application (CNQX/D-AP5 and gabazine in (A) or only gabazine in (B)). Red crosses indicate outliers. Striatal neurons were patched with either Cs^+

internal solution at a holding potential of +40 mV or with high Cl^- internal solution at a holding potential of -70 mV. Data were pooled since there was no statistical difference between the two conditions.

(C) Representative reconstruction of a responding SPN (axon in red) following photostimulation, and bright field image of dendritic spines.

(D) PSCs of responding GABAergic interneuron at 40 mV, at reversal potential of -75 mV and at -95 mV holding potential with Cs^+ internal solution.

(E) Epifluorescence images of representative M1 (left) and M2 (right) injection sites inserted in schematic drawings of coronal sections.

(F) Exemplary DIC and epifluorescence images of iSPNs that responded to photostimulation and were located in proximity to $mCherry^+$ long-range projections.

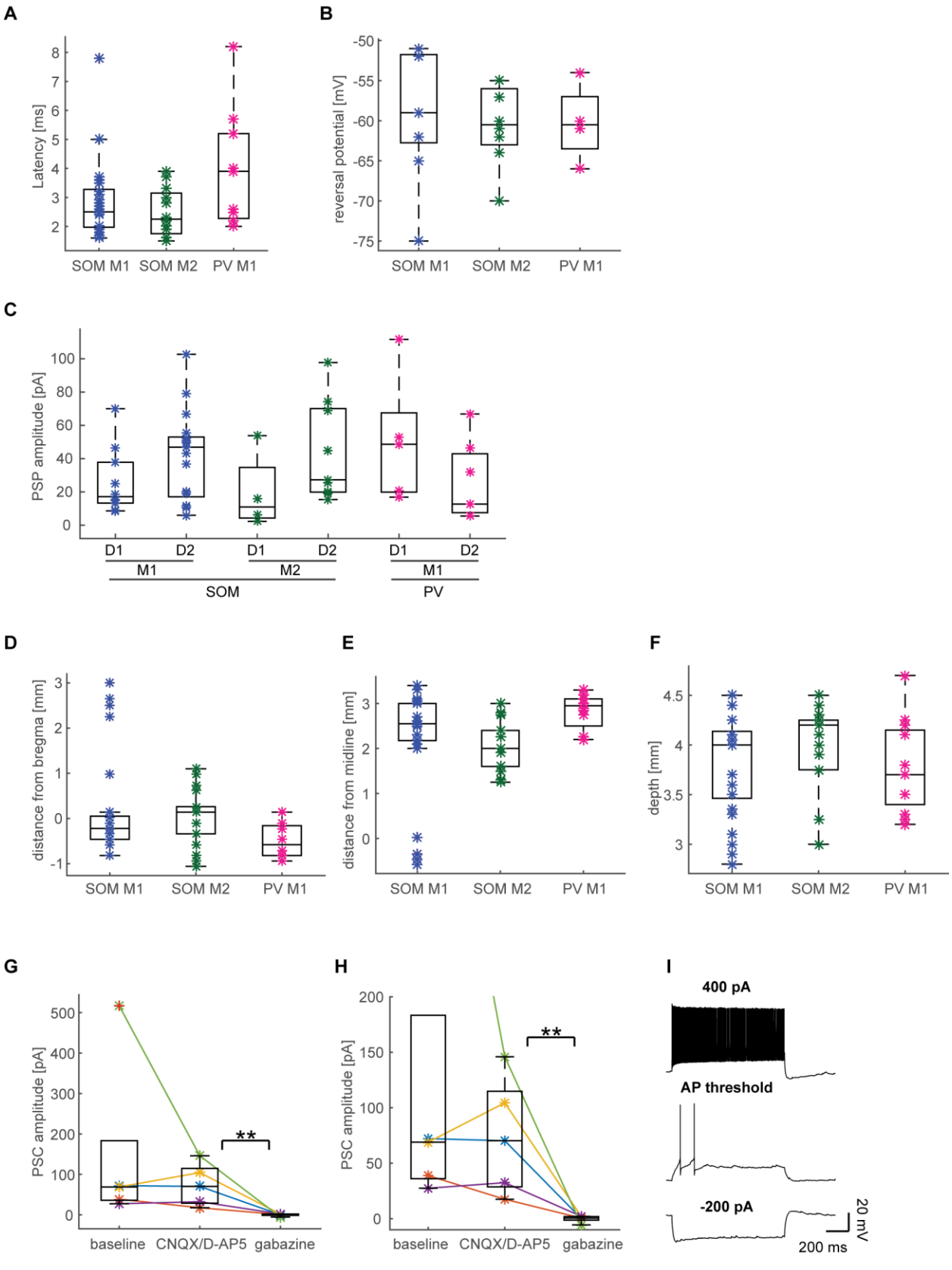
A
Latency [ms]
SOM M1
SOM M2
PV M1
B
reversal potential [mV]
SOM M1
SOM M2
PV M1
C
PSP amplitude [pA]
D1
D2
M1
M2
SOM
PV
D
distance from bregma [mm]
SOM M1
SOM M2
PV M1
E
distance from midline [mm]
SOM M1
SOM M2
PV M1
F
depth [mm]
SOM M1
SOM M2
PV M1
G
PSC amplitude [pA]
**
baseline
CNQX/D-AP5
gabazine
H
PSC amplitude [pA]
**
baseline
CNQX/D-AP5
gabazine
I
400 pA
AP threshold
-200 pA
20 mV
200 ms

Figure S3 (related to Figure 2 and 3)

Responses of SPNs upon stimulation of motor cortex SOM^+ and PV^+ neuron projections are similar

(A-B) Dot/box plots (median (IQR), range) for latency (A) and reversal potential (B) of striatal SPN responses upon photostimulation of primary motor cortex (M1) SOM^+ and PV^+ neuron projections as well as secondary motor cortex (M2) SOM^+ neuron projections.

(C) Dot/box plots for the PSC amplitudes in direct (D1) and indirect (D2) SPNs upon photostimulation of M1 SOM^+ and PV^+ neuron projections as well as M2 SOM^+ neuron projections. Striatal neurons were patched with Cs^+ internal solution and clamped at 0 mV holding potential.

(D-F) Dot/box plots for the coordinates of the localization of responding SPNs in striatum.

(G-H) Dot/box plots indicating the PSC amplitudes of striatal target neurons upon photostimulation of PV^+ neuron projections before (baseline) and after drug (CNQX/D-AP5 and gabazine) application. Striatal neurons were patched with high Cl^- internal solution at a holding potential of -70 mV. Red cross indicates outlier. (H) Magnification of (G) to highlight changes upon gabazine application.

(I) Firing pattern of a fast spiking PV^+ projecting neuron identified by retrograde tracing with SADΔG-EGFP(EnvA) rabies virus. TCB was expressed Cre-dependently in the motor cortex of PV^{Cre} mice and rabies virus was injected into striatum.

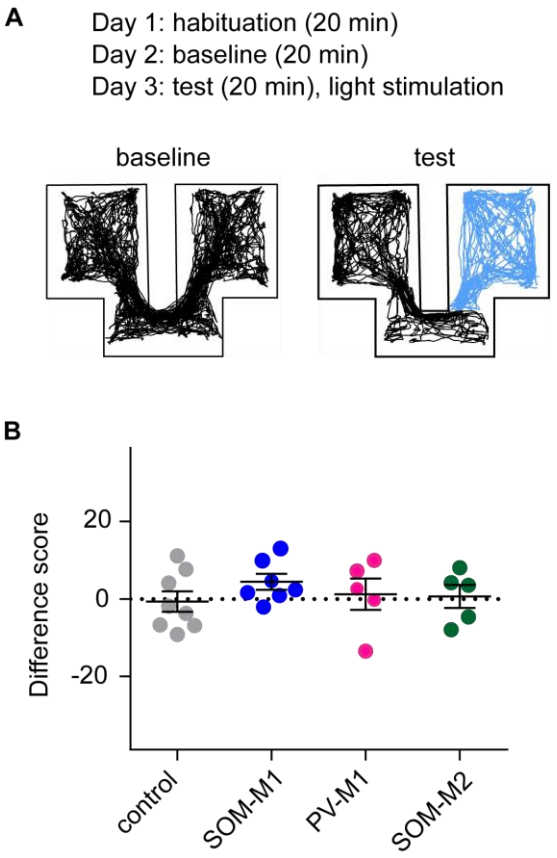

Figure S4 (related to Figure 4)

Stimulation of striatal long-range projections of motor cortex PV$^+$ and SOM$^+$ neurons does not elicit place preference

(A) Exemplary motion traces during baseline and test phases of the light-mediated place preference assay. In the baseline phase, locomotion was measured without photostimulation. During test phase, entering one of the compartments (stimulation side, blue trace) elicited photostimulation.

(B) Mean (± SEM) difference score, as the % of time spent on the 'stimulation' side during baseline minus the % of time spent on the same side during test. Control: n = 8, SOM-M1: n = 7, PV-M1: n = 5, SOM-M2: n = 5 mice.

SUPPLEMENTAL TABLES

Table S1 (related to Figure 1)

Motor cortex SOM$^+$ neurons project to several cortical and subcortical brain areas.

Injection site	Cortical target areas	Subcortical target areas
M1 (n=3)	AI, DI, FrA, GI, M2, S1 DLO, PrL, S2 Cg1/2, Ect, Au2, TeA, LO, LPtA, cl M1, VO	ac, cc, **CPu**, IPAC, LGP acp, ec, ic AA, cg, cl, I, MCLH, MCPO, MGP, rt, Tu, VL, VM, VP
M2 (n=4)	FrA, M1, PrL Cg, DLO, DP,LO, MO, S1, S2, VO AI, cl DP, cl M2, DI, GI, IL, LPtA/MPtA, Pir, V1, V2	cc, **CPu** DTT, LGP, LS, SL, Tu, AAV, cl, ec, HDB, ic, ICj, MGP, MS, Rt, SHi, VDB

Color code indicates areas where labeled projections from M1 and M2 were found in all (magenta), at least 2 (green) or only 1 (blue) injected mouse. The dorsal striatum (CPu, caudate putamen) is highlighted with bold letters. Brain areas were identified based on the Paxinos mouse brain atlas.

Abbreviations cortical areas: **AI**, agranular insular Cx; **Au2**, secondary auditory Cx; **Cg**, cingulate Cx; **cl**, contralateral; **DI**, dysgranular insular Cx; **DLO**, dorsolateral orbitofrontal Cx; **DP**, dorsal peduncular Cx; **Ect**, ectorhinal Cx; **FrA**, frontal association area; **GI**, granular insular Cx; **IL**, infralimbic Cx; **LO**, lateral orbitofrontal Cx; **LPtA**, lateral parietal association Cx; **M1**, primary motor Cx; **M2**, secondary motor cortex; **MO**, medial orbitofrontal Cx; **MPtA**, medial parietal association Cx; **Pir**, piriform Cx; **PrL**, prelimbic Cx; **RSA**, retrosplenial agranular Cx; **S1**, primary somatosensory Cx; **S2**, secondary somatosensory Cx; **TeA**, temporal association Cx; **V1**, primary visual Cx; **V2**, secondary visual Cx; **VO**, ventral orbitofrontal Cx;

Abbreviations subcortical areas: **AA**, anterior amygdaloid area; **AAV**, ventral anterior amygdaloid area; **ac**, anterior commissure; **acp**, anterior commissure, posterior; **cc**, corpus callosum; **cg**, cingulum; **cl**, claustrum; **CPu**, caudate putamen / dorsal striatum; **DTT**, dorsal tenia tecta; **ec**, external capsule; **HDB**, horizontal diagonal band of Broca; **I**, intercalated ncl of the amygdala; **ic**, internal capsule; ICj, island of Calleja; **IPAC**, interstitial nucleus of the posterior limb of the anterior commissure; **LGP**, lateral globus pallidus; **LS**, lateral septum; **MCPO**, magnocellular preoptic ncl; **MGP**, medial globus pallidus; **MS**, medial septum; **Rt**, reticular thalamic ncl; **SHi**, septohippocampal ncl; **SL**, semilunar ncl; **Tu**, olfactory tubercle; **VDB**, ventral diagonal band of Broca; **VL**, ventrolateral thalamic ncl; **VM**, ventromedial thalamic ncl; **VP**, ventral pallidum.

Table S2 (related to Figure 1 and 3)

Firing properties of motor cortex SOM$^+$ and PV$^+$ projecting neurons

	SOM projecting (n = 11)	SOM non-projecting$^-$ (n = 14)	Non-pyramidal PV projecting (n = 3)	Statistics (SOM projecting vs. non-projecting)
V_m [mV]	-63.2 ± 1.6	-66.1 ± 2.1	-63.4 (3.0)	p = 1 $t_{(22)}$ = 1.0
R_i [MOhm]	127.0 (26.4)	136.5 (54.2)	102.9 ± 4.7	p = 1 U = 67
AP_{th} [mV]	-39.3 (3.6)	-38.5 (8.0)	-33.2 (6.8)	p = 1 U = 48.5
Rheobase [pA]	84.0 ± 6.5	144.3 ± 20.5	173.3 ± 40.7	p = 0.12 $t_{(15.6)}$ = 2.8
$AP_{1/2}$ [ms]	0.66 ± 0.04	0.52 ± 0.02	0.37 ± 0.01	p = 0.10 $t_{(12.7)}$ = 3.0
AP_{amp} [mV]	50.1 ± 3.6	54.8 ± 3.1	46.6 ± 2.7	p = 1 $t_{(22)}$ = 1.0
F_{max} [Hz]	120.5 (43.0)	149.5 (84.0)	232.0 (60)	p = 1 U = 38
I_{max} [pA]	342.5 ± 53.8	540 ± 53.1	680 ± 33.5	p = 0.17 $t_{(20)}$ = 2.4
Sag [%]	27.6 ± 5.8	10.2 ± 1.6	17.0 ± 4.9	p = 0.12 $t_{(10.4)}$ = 2.9
Total adaptation [%]	47.9 (28.7)	39.2 (31.3)	34.7 (9.6)	p = 1 U = 42

Retrogradely labeled RbV-EGFP and TCB positive neurons were patched in motor cortex of *SOM^{Cre}* and *PV^{Cre}* mice. Firing patterns were recorded in whole-cell mode with low Cl^- intracellular solution. No statistically significant differences were found between SOM cells that were retrogradely labeled as compared to those that expressed TCB but not RbV-EGFP.

Data are shown as median (IQR) or mean ± SEM. Comparisons were made using Mann-Whitney-U test or unpaired t-test. P-values were corrected for familywise errors using the Holm-Bonferroni test.

Table S3 (Related to Figure 2 and S2)

Electrophysiological properties of target cells and non-targeted SPNs.

	Target SPNs (n = 13)	Non-target SPNs (n = 34)	Cholinergic interneurons (n = 10)	GABAergic interneuron (n = 1)	Statistics (target vs. other SPNs)
V_m [mV]	-79.9 (7.0)	-79.8 (7.7)	-55.2 (9.0)	-63	p = 1 U = 216
R_i [MOhm]	82.0 (34.2)	87.2 (48.6)	181.1 (56.0)	249	p = 1 U = 179
AP_{th} [mV]	-41.0 ± 0.8	-39.2 ± 0.7	-44.6 ± 1.6	43	p = 0.96 $t_{(45)}$ = 1.45
Rheobase [pA]	230 (145)	200 (120)	0 (10)	30	p = 1 U = 196
$AP_{1/2}$ [ms]	0.76 (0.10)	0.85 (0.13)	1.34 (0.40)	0.3	p = 0.48 U = 142
AP_{amp} [mV]	91.5 (9.8)	86.5 (8.8)	71.1 (10.7)	85	p = 0.96 U = 158
F_{max} [Hz]	56.5 ± 6.6	59.7 ± 2.9	20.5 ± 2.4	191	p = 1 $t_{(42)}$ = 0.49
I_{max} [pA]	750 (425)	820 (360)	270 (180)	690	p = 1 U = 180

Cells were patched with high Cl^- intracellular solution. Electrophysiological properties of target and non-target SPNs did not differ. Data are shown as median (IQR) or mean ± SEM. Comparisons were made using Mann-Whitney-U test or unpaired t-test; p-values were corrected for familywise errors using the Holm-Bonferroni test.

Table S4 (Related to Figure 2 and 3)

Response properties and localization of SPNs targeted by M1 and M2 SOM$^+$ and PV$^+$ projecting neurons.

	SOM-M1	SOM-M2	PV-M1	Statistics SOM-M1 vs. SOM-M2	Statistics PV-M1 vs. SOM-M1
Distance from midline [mm]	2.55 (0.8) n = 25	2.0 (0.8) n = 16	3.0 (0.6) n = 12	p = 0.04 U = 142	p = 0.07 U = 95
Distance from bregma [mm]	-0.2 (0.5) n = 25	0.1 (0.6) n = 16	-0.6 (0.7) n = 12	p = 0.3 U = 152	p = 0.02 U = 81
Depth [mm]	4.0 (0.7) n = 25	4.2 (0.5) n = 16	3.7 (0.8) n = 12	p = 0.07 U = 152	p = 0.8 U = 142
Amplitude [pA]	37 (36.6) n = 27	25.4 (41.9) n = 13	26.6 (38.1) n = 12	p = 0.93 U = 172	p = 0.8 U = 152
Latency [ms]	2.5 (1.3) n = 25	2.25 (1.4) n = 12	3.90 (2.93) n = 11	p = 0.4 U = 124	p = 0.08 U = 87
Reversal potential [mV]	58.4 ± 2.7 n = 9	-60.5 ± 1.8 n = 8	-60.3 ± 2.5 n = 4	p = 0.5 $t_{(15)}$ = 0.62	p = 0.7 $t_{(11)}$ = -0.4

Data are shown as median (IQR) or mean ± SEM. Comparisons were made using Mann-Whitney-U test or unpaired t-test.

SUPPLEMENTAL EXPERIMENTAL PROCEDURES

All experiments were performed in 8 to 20 weeks old male *SOM*^{Cre} (Melzer et al., 2012), *PV*^{Cre} (Hippenmeyer et al., 2005), *PV*^{Cre}/GAD67-EGFP (Tamamaki et al., 2003), *SOM*^{Cre}/DRD1a-EGFP, *PV*^{Cre}/DRD1a-EGFP, *SOM*^{Cre}/DRD2-EGFP (Gong et al., 2003) and *PV*^{Cre}/DRD2-EGFP mice with a C57BL/6 background. Animals used for tracing experiments and electrophysiological recordings were group-housed, animals used for behavioral experiments were single-housed. All mice were kept on a 12 h light/dark cycle. All experiments were conducted during the light phase of the schedule.

AAV injections

The pAAV-double floxed-hChR2(H134R)-mCherry-WPRE-pA (AAV DIO *ChR2-mCherry*) vector was obtained from Karl Deisseroth (Cardin et al., 2010). The vector carries an inverted version of Channelrhodopsin2 fused to the fluorescent marker mCherry. In the presence of Cre recombinase, the cassette is inverted into the sense direction, and the fused proteins are expressed from the EF1 promoter. AAV chimeric vectors (virions containing a 1:1 ratio of AAV1 and AAV2 capsid proteins with AAV2 ITRs) were generated as previously described (Klugmann et al., 2005). All rAAVs were stored in undiluted aliquots at a concentration $>10^{12}$ genomic copies per ml at −80° C until intracranial injections were performed.

We injected 8 weeks old male *SOM*^{Cre}, *PV*^{Cre}, *PV*^{Cre}/GAD67-EGFP, *SOM*^{Cre}/DRD1a-EGFP, *PV*^{Cre}/ DRD1a-EGFP, *SOM*^{Cre}/DRD2-EGFP, *PV*^{Cre}/ DRD2-EGFP and *SOM*^{Cre}/*GAD67*^{EGFP} mice. Anesthesia was induced and maintained with isoflurane (1-2.5%). For injections, a small craniotomy (~ 1 mm diameter) was made using the following coordinates (distance from bregma [mm] / distance from midline [mm] / depth [mm] / angle):

Combined primary/secondary motor cortex: 1.8 / 1.5 / 0.7 / 2 degrees towards front

Primary motor cortex: 1.1 / 1.9 / 0.7 / 2 degrees towards front

Secondary motor cortex: 1.6 / 0.8 / 0.6 / 2 degrees towards front

Virus was delivered through a small durotomy by a glass micropipette with a tip resistance of 2 to 4 MOhm. A volume of 100 nl virus (AAV DIO *ChR2-mCherry*) was injected. For more specific injections into primary or secondary motor cortex, 50 nl virus was used. The virus titre was $2x10^{15}$ virus genome/ml, and the pipette held in place for 7 min. The pipette was retracted 50 µm towards the surface, and held in place for another 2 min before complete retraction from the brain. The scalp incision was sutured, and post-surgery analgesics were given to aid recovery (0.03 mg/kg KG Metamizol). Mice were housed for three weeks following the surgery.

Immunohistochemistry

Mice were transcardially perfused with 4% paraformaldehyde (PFA). Coronal and sagittal sections were cut at 50 or 150 µm thickness on a vibratome and washed with phosphate buffered saline (PBS). Free-floating sections were permeabilized and blocked for 2 hrs with PBS containing 5% BSA and 0.2% Triton X-100. Incubation of the sections with primary antibodies was performed for 48 hrs at 4°C. For double-labeling experiments both primary antibodies were incubated simultaneously. Sections were washed with PBS and incubated for 2 hrs with Cy3-conjugated secondary antibody (Jackson Immunoresearch, Newmarket, UK, 1:1000) and/or AlexaFluor488 anti-rabbit secondary antibody (Invitrogen, Darmstadt, Germany, 1:1000) and/or AlexaFluor488 anti-chicken secondary antibody (Life Technologies, Darmstadt, Germany, 1:1000). After repeated washing with PBS, the sections were mounted on 0.1% gelatin-coated glass slides using Mowiol 40-88. Pictures were taken using a BX 51 microscope and a confocal laser-scanning microscope. All injection sites were carefully examined, and mice with labeling of cell bodies in other brain areas were excluded from analysis.

Primary Antibodies

Rabbit anti-somatostatin (Millipore, Temecula CA, 1:1000); rabbit anti-Ds-red (Clontech, Mountain View CA, 1:1000); rabbit anti-EGFP (Invitrogen, Darmstadt, Germany, 1:5000); chicken anti-EGFP (Invitrogen, Darmstadt, Germany, 1:1000); rat anti-somatostatin (Millipore, Temecula CA, 1:500), chicken anti-EGFP (Abcam, Cambridge MA, 1:1000).

DAB staining

Sections were quenched in 1% H_2O_2 for 10 min followed by thorough washing with PBS, before being permeabilized with 1% Triton X-100 in PBS for 1 hr. After repeated washing, sections were incubated with avidin-biotin-horseradish peroxidase complex (Elite ABC, Vector Laboratories, Burlingame CA) in PBS over night at 4°C. After washing with PBS, sections were incubated in a solution containing 0.04% DAB, 49.6% ammonium chloride buffer (0.08% ammonium chloride in PB), and 0.4% glucose oxidase to which 10% beta-D-glucose in H_2O (20 µl/ml) was added one minute after start of the reaction. Sections were kept in the dark for 15-45 min. The reaction was stopped by washing sections again in PBS. Sections were mounted on glass slides using Mowiol 40-88.

Retrograde tracer injection

Seven to10 weeks old wildtype mice were injected into the striatum with 250 nl CTB 647 (4 µg/µl) (Molecular Probes, Eugene, OR). Surgery was as described above. CTB was injected with a flow rate of 100 nl/min using a UMP3 microsyringe pump (World Precision Instruments, Sarasota FL). The pipette was held in place for 10 min before being slowly retracted from the brain within 20 min. The coordinates were (in mm) -2 AP / 2.9 ML / 4 deep with an angle of 30 degrees towards the front. We found that these coordinates were essential to prevent the injection pipette from crossing cortical areas that receive long-range GABAergic inputs from motor cortex, and thus to prevent erroneous labeling of corticocortical GABAergic projecting neurons. 12-14 days after injection mice were sacrificed, sectioned on a cryostat and used for *in situ* hybridization.

Rabies virus tracing

EnvA-pseudotyped, glycoprotein-deleted rabies virus carrying EGFP transgene (SADΔG-EGFP(EnvA)) was generated in house, using starting materials from Byung Kook Lim (UCSD). The recombinant rabies viruses were generated using BHK-B19G and BHK-EnvA cells using protocols similar to those previously described (Wickersham et al., 2010), and were used at a titer of approximately 1.0 x 10^9 infectious units/ml.

Fourteen to 15 weeks old A2A-Cre mice were injected into the striatum with 300-400 nl AAV9 packaged with CAG-Flex-TCB (virus titer $1.5x10^{13}$ gc/ml) encoding the avian virus receptor fused to mCherry, and CAG-Flex-RG ($8.7x10^{13}$ gc/ml) encoding the rabies glycoprotein. Plasmids were a gift from Liqun Luo (Addgene plasmids # 48332 and # 48333). Surgery was as described above. The pipette was held in place for 10 min before being slowly retracted from the brain within another 20 min. The coordinates were (in mm) 0 AP, 2.9 ML, 3.5 deep. 3 weeks later, 400-500 nl rabies viruses were injected in the striatum as described above. Coordinates were either the same as for the AAVs or -2 AP, 2.9 ML, 4 deep with 30 degree angle towards the front. Mice were sacrificed 10 days later and brains were sectioned on a cryostat for subsequent *in situ* hybridization.

To specifically label SOM^+ and PV^+ projecting neurons, we injected 400 nl AAV2/DJ packaged with CAG-Flex-TCB (plasmid as above, virus titer $1x10^{13}$ gc/ml) into the primary and secondary motor cortex (coordinates as above) of SOM^{Cre} ($Sst^{tm2.1(cre)Zjh}$, Jackson Laboratory) and PV^{Cre} mice. The pipette was held in place for 5 min before injecting. AAVs were injected with 50 nl/min flow rate and the pipette retracted 10 min after injection. 2 weeks later, 400 nl SADΔG-EGFP(EnvA) were injected into the striatum with the following coordinates (in mm): -2.6 AP, 2.8 ML 4 and 4.5 deep with 35 degrees angle towards the front. Mice were sacrificed 8-9 days later and used for immuncytochemstry against EGFP and SOM or electrophysiology to characterize electrophysiological parameters of projecting neurons. Since few pyramidal cells were also labeled after injections of the same AAV and rabies virus into C57/BL6 wiltype mice, we assumed that this AAV had Cre-independent 'leak' expression in pyramidal cells, and we thus limited our analysis to cells that had strong TCB-mCherry expression. In SOM^{Cre} mice all patched TCB/$EGFP^+$ cells were non-pyramidal, in PV^{Cre} mice, 1 out of 4 cells had a cell body shape and firing properties of pyramidal cells and was thus excluded from firing pattern analysis.

Three hemispheres of 3 mice were used to exclude that labeling arose from pipette track in cortex. These mice were injected with the same CTB/rabies mixture and the same coordinates except that the rabies injection site was 1.2 mm deep and only 200 nl were injected. No retrograde labeling was observed in the motor cortex of in these mice suggesting that our labeling was specific for striatal injections.

Morphological reconstruction

For morphological reconstruction of projecting neurons, brains were fixed overnight in 4% PFA, coronal slices of 75 µm were cut on a vibratome. Only mice with sparse retrograde labeling (1-2 cells per hemisphere) were used so that

dendrites and axons could be clearly assigned to the reconstructed cell. Slices with retrogradely labeled cell bodies and up to 3 slices anterior and posterior of the cell body were immunostained for EGFP and SOM. In brief, slices were washed in PBS, incubated in PBS with 5% NGS and 0.2% Triton for 1 hr and then incubated at 4°C for 24 hrs with rat anti-SOM and chicken anti-EGFP antibodies. Slices were then washed in PBS with 0.2% Triton, followed by incubation with secondary antibody Alexa 488 anti-chicken and Alexa 647 anti-rat for 1 hr at RT. Slices were washed in PBS with 0.2% Triton followed by PBS.

For morphological reconstructions, only cells that were clearly TCB, EGFP and SOM positive were chosen. Stacks (15 images) of up to 7 consecutive slices surrounding and including the cell body were imaged on a Leica SP8 X confocal microscope using a 20x 0.75 NA oil immersion Leica objective (Leica, Wetzlar, Germany). Tile stack images were merged and maximal intensity projections constructed in Leica Application Suite X software. Cells were reconstructed in Adobe illustrator CS5.

Fluorescent *in situ* hybridization

Mice were deeply anesthetized with isoflurane and decapitated, and their brains were quickly removed and frozen in Tissue Tek OCT compound (VWR, Radnor PA) on dry ice. Brains were cut on a cryostat (Leica CM 1950) into 20 µm sections, adhered to SuperFrost Plus slides (VWR, Radnor PA), and immediately refrozen. Samples were fixed in 4% paraformaldehyde for 15 min at 4 degrees, processed according to RNAscope Fluorescent Multiplex Assay manual (Advanced Cell Diagnostics, Newark CA), and coverslipped with ProLong antifade reagent (Molecular Probes, Eugene, OR). *Gad1* and *Gad2* probes were combined in one channel.

Image analysis

For quantification of retrogradely labeled neurons, 20 µm thick coronal cryostat sections stained with *in situ* hybridization were used. The whole motor cortex of 34 slices was searched for retrograde labeling in rabies virus injected mice using a Leica SP8 X confocal microscope equipped with a 63x 1.4 NA oil immersion objective (Harvard NeuroDiscovery Center). For CTB injected mice, 35 sections were imaged on a Leica SP8 X confocal microscope using a 63x 1.4 NA oil immersion objective (Harvard NeuroDiscovery Center). Per section, one tiled image of 530+/- 10 µm width covering all layers (average are: 530.75 x 1554.06 µm) of the motor cortex was obtained with autofocus, a pixel size of 180 nm and an optical section of 0.9 µm. Imaging sites were chosen such that they were consistent with our anterograde virus injections.

Laser power/intensity for *in vitro* and *in vivo* experiments

Laser power at the optical fiber tip was measured with an optical power meter (POM-110, OZ Optics Ltd., Carp, Canada). For our *in vitro* setup power was ~3.7 mW and for our *in vivo* setup ~3.0 mW. Used fibers were 200 µm in diameter, resulting in a laser intensity (or accurately speaking the irradiance) at the tip of our optic fiber of ~118 mW/mm^2 and ~95 mW/mm^2 for our *in vitro* and *in vivo* setup, respectively. For an estimation of the intensity within the tissue we used: http://web.stanford.edu/group/dlab/cgi-bin/graph/chart.php.

Electrophysiological recordings

For *in vitro* patch-clamp recordings, mice were deeply anesthetized with inhaled isoflurane, and transcardially perfused with ~30 ml ice-cold sucrose solution oxygenated with carbogen gas (95% O2, 5% CO2, pH 7.4). Mice were decapitated and brains removed. 300 µm thick sections were cut on a slicer in ice-cold oxygenated sucrose solution containing (in mM) 252 sucrose, 3 KCl, 1.25 $Na_2H_2PO_4$, 24 $NaHCO_3$, 2 $MgSO_4$, 2 $CaCl_2$, 10 glucose. First, coronal, sagittal and horizontal slices were used. For experiments comparing M1 vs. M2 only coronal slices were used. Slices were incubated in oxygenated Ringer's extracellular solution containing (in mM) 125 mM NaCl, 25 mM $NaHCO_3$, 1.25 mM NaH_2PO4, 2.5 mM KCl, 2 mM $CaCl_2$, 1 mM $MgCl_2$, 25 mM glucose at 32 °C for ~15 min, and subsequently at RT until used for recordings. Whole-cell patch-clamp recordings were performed at 30-32° C using pipettes pulled from borosilicate glass capillaries with resistances of 3-5 MΩ. Sections were continuously perfused with oxygenated extracellular solution. Cells were visualized by an upright microscope equipped with infrared-differential interference contrast and standard epifluorescence.

To investigate synaptic inputs, axonal fibers were stimulated with blue laser light. PSCs were recorded in response to 5 ms photostimulations (473 nm) using approximately 120 mW/mm^2 laser intensity. Glutamatergic and GABAergic synaptic inputs were tested adding via bath-application the following pharmacological agents: Gabazine (10 µM; SR 95531 hydrobromide), D-AP5 (50 µM) and CNQX (10 µM). Amplitudes and latencies of PSCs were measured at 0

mV holding potential using Cs^+-based intracellular solution containing (in mM) 120 Cs^+- gluconate, 10 CsCl, 10 Hepes, 10 phosphocreatine, 8 NaCl, 2 Mg-ATP, 0.3 GTP and 0.2 Hepes, pH 7.3 adjusted with CsOH. FitMaster (HEKA, Lambrecht, Germany) was used for offline analysis of PSCs. In some cases K^+-based, high Cl^- intracellular solution containing (in mM) 127.5 KCl, 11 EGTA, 10 Hepes, 1 $CaCl_2$, 2 $MgCl_2$, 2 Mg-ATP and 0.3 GTP, pH 7.3 adjusted with KOH was used to record firing patterns in targeted cells. In these cases, PSCs were measured at -70 mV holding potential. PSCs were defined as deflections that were time locked to the stimulation and that were larger than the spontaneous fluctuations that occurred during baseline recorded before stimulation after averaging all traces of an experiment. The amplitude is thus measured as difference between amplitude of time-locked deflection and amplitude of spontaneous changes and cells with an amplitude >0 pA were considered as responding. All cells with responses >0 pA were included in the dot plot graphs.

Firing patterns were analyzed in current clamp mode applying 1 s current pulses with 3 s intersweep interval, starting at -50 pA (striatum) or -200 pA (retrogradely labeled cells in motor cortex) and gradually increasing the amplitude in 20 pA steps until saturation was reached. Interpulse interval was set to 3 s. Saturation was defined as a decrease in action potential amplitudes. Firing patterns were analyzed off-line using Matlab. Input resistance was calculated from the steady state voltage step to the first hyperpolarizing current injection for 1 s. Action potential half width was measured at half amplitude of the AP. Maximal frequency was measured at 1000 pA current injection or directly before saturation of the cell. Rheobase was calculated as the minimal injected current that is required to elicit action potentials in whole-cell mode.

For distinction of dSPNs and iSPNs and for comparison of M1 and M2 injections, dSPNs, iSPNs cholinergic and GABAergic interneurons were patched in DRD1a-EGFP and DRD2-EGFP mice cross-bred to either SOM^{Cre} or PV^{Cre} mice. Cholinergic and GABAergic interneurons were patched also in SOM^{Cre} and PV^{Cre} mice since their identification did not require EGFP labeling.

In brief, cell classification into SPNs, cholinergic and GABAergic interneurons in wildtype mice was based on the following characteristics: Cholinergic cells were detected based on their large cell somata, their depolarized resting membrane potential and their slow action potential firing. SPNs and GABAergic interneurons were mostly medium sized and clearly distinguishable from cholinergic cells based on their electrophysiological properties: both cell types are more hyperpolarized and have a higher maximal firing frequency. While GABAergic interneurons can be fast-spiking or non-fast spiking, SPNs are characterized by typical ramp depolarization before action potential initiation, followed by regular action potential firing.

Series resistance was continuously monitored in voltage-clamp mode during PSC recordings measuring peak currents in response to small hyperpolarizing pulses. Series resistances of 37 MOhm were accepted for analyzing PSCs. Stimulus delivery and data acquisition was performed using Pulse software. Signals were filtered at 3 kHz, sampled at 10 kHz. Liquid junction potentials were not corrected.

Biocytin filling and cell reconstruction

For morphological analysis of electrophysiologically identified target cells, whole-cell patch-clamped neurons were filled with biocytin (Aldrich, Taufkirchen, Germany; 10 mg/ml, dissolved in intracellular solution). Cells were filled for up to 30 min before retracting the pipette. The slices with filled cells were fixed overnight in 4% paraformaldehyde and stained with DAB as described above. Labeled cells were reconstructed using Neurolucida software (MicroBrightField, Colchester VT).

Behavioral experiments

Surgery: We bilaterally injected AAV-DIO *ChR2-mCherry* into M1 or M2 of SOM^{Cre} mice and into M1 of PV^{Cre} mice (henceforth, SOM-M1, SOM-M2 and PV-M1 experimental groups, respectively). The control group included: SOM^{Cre} and PV^{Cre} mice injected with AAV1.EF1a.DIO.eYFP.WPRE.hGH (AVV-DIO eYFP) (PennVector, Deisseroth lab) and wildtype litter-mates injected either into the M1 or M2 with AAV-Syn *Tomato* (where the synapsin promoter directs the expression of the fluorescent protein Tomato). Data from these 3 groups of control mice was pooled since no difference in performance was found (data not shown). Viral injections were performed as described above. After injections, we bilaterally implanted optic fiber cannulas (diameter: 200 µm, NA: 0.37, Doric lenses, Quebec, Canada) into the striatum (0.2 mm posterior from bregma, ± 2.8 mm lateral from the midline and 3 mm deep). All mice were male and between 11-17 weeks old when surgery was performed. Mice were single-housed for 3-4 weeks following surgery before behavioral experiments started.

Behavioral set up and protocols: In all experiments, mice were video-tracked at 25 frames per sec and their movements subsequently analyzed using a position tracking system (Ethovision XT9, Noldus). The implanted optic fiber cannulas were connected to two optic fibers attached to a rotary joint (Doric lenses, Quebec, Canada). A patch cord connected the optic fibers to a diode-pumped solid-state 473-nm laser (CrystaLaser, Reno NV). We used a pulse generator (Master 8) and a TTL control box (USB-IO box, Noldus) to automatically control the photostimulation (5 ms pulses delivered at 20 Hz. Laser power, 3 mW).

Evaluation of locomotion activity was performed in a circular arena (40 x 40 cm) placed in a dim lighted room. Animals were allowed to freely run for 21 min. Animals were first recorded for 5 min before any photostimulation. Photostimulation lasted 2 min and was repeated 3 times with an inter-stimulation period of 4 min. The photostimulation protocol can be summarized as follows: 5 min no stimulation, 2 min photostimulation, 4 min no stimulation, 2 min photostimulation, 4 min no stimulation, 2 min photostimulation, 2 min no stimulation. Raw data obtained every 40 ms were processed as follows. We first calculated the distance moved during 5 s (henceforth, "motion"), second we calculated the difference between median motion during and before photostimulation for four epochs of different durations, i.e., 10, 30, 60 and 120 s, starting at photostimulation onset (the median was considered as the data was non normally distributed). Baseline was calculated as the median motion during 120s before photostimulation. For each time epoch we averaged the values obtained during the 3 stimulation periods so that we obtained one single value per mouse. Cumulative frequency histograms as well as mobility and immobility bouts were calculated using the distance moved during 1s windows. Mobility bouts were defined as events in which the average speed (for any 1 s window) was ≥ 1cm/s. Immobility bouts were defined as events in which the average speed (for any 1 s window) was < 1cm/s.

For the place preference task we used a box containing two 20 x 20 x 35 cm compartments connected by a neutral chamber (10 x 20 x 35 cm). Each compartment had distinctive wall patterns (white circles against a black background vs. black circles against a white background). The assay consisted of three 20 min sessions over 3 days. Each session started with the mouse placed into the neutral chamber. We recorded the movements of the mouse inside the two compartments. On day 1, mice were habituated to the apparatus. On day 2 (baseline), no photostimulation was presented. On day 3 (test), one compartment was randomly designated to trigger photostimulation after entry ("stimulation side"). The position of the mouse was calculated in real time using Ethovision software, and this position was used to control the onset of the laser. The sides of the stimulated compartments were counterbalanced across all mice. We first measured the percentage of time spent in each compartment and then calculated a difference score as the percentage of time spent in the "stimulation side" during baseline minus the percentage of time spent on the same side during test (time spent in the neutral chamber connecting both compartments was not considered). A difference score > 0 indicates avoidance of the stimulation side, while a difference score < 0 indicates preference to the stimulation side.

Histology: At the end of the experiments, mice were transcardially perfused with PBS and paraformaldehyde as described above. Brains were dissected and sliced on a vibratome (VT1000s vibratome, Leica, Germany) into 150 µm thick coronal slices. DAB staining was performed as described above to confirm injection and implantation sites.

Statistics

We did not perform blind experiments and did not use statistical methods to predetermine sample size, however, our sample sizes are similar to those generally employed in the field. For electrophysiological data, the Shapiro-Wilk test was used to test for normal distribution. Normally distributed data were then tested for homogeneity of variance using F-tests and data were compared using unpaired t-tests either for equal or unequal variance. Group pairs with at least one non-normally distributed dataset were compared using Mann-Whitney-U tests. Variables for which all groups were normally distributed are shown as mean ± SEM. Variables for which at least one group was non-normally distributed are shown as median (IQR). Proportions of targeted cells were compared using Fisher's exact tests. For pairwise comparisons, paired t-tests (normally distributed data) or Wilcoxon signed rank tests (non-normally distributed data) were used. For multiple pairwise comparisons, Friedman test followed by *post hoc* Conovor's tests (non-normally distributed data) were used. P-values for all multiple electrophysiological and pharmacological data and proportions were corrected with the Holm-Bonferroni test to control for familywise error rates.

For behavioral data, Shapiro-Wilk and Brown-Forsythe tests were used to test normality and homogeneity of variances, respectively. Motion difference for each time window and the difference score were compared across groups using a one-way ANOVA followed by Tukey's multiple comparisons tests. Mobility and immobility bouts before and during photostimulation were compared using paired t-test and Wilcoxon matched-pairs signed rank test.

Graphs were made with Excel (Microsoft), Matlab (The MathWorks) and Prism 6 (GraphPad). The figures were assembled in Illustrator (Adobe) and Inkscape.

The following code was used for p-values in our figures: * < 0.05; ** < 0.01; *** < 0.001.

SUPPLEMENTAL REFERENCES

Cardin, J.A., Carlén, M., Meletis, K., Knoblich, U., Zhang, F., Deisseroth, K., Tsai, L.-H., Moore, C.I., 2010. Targeted optogenetic stimulation and recording of neurons in vivo using cell-type-specific expression of Channelrhodopsin-2. Nat. Protoc. 5, 247–254.

Klugmann, M., Symes, C.W., Leichtlein, C.B., Klaussner, B.K., Dunning, J., Fong, D., Young, D., During, M.J., 2005. AAV-mediated hippocampal expression of short and long Homer 1 proteins differentially affect cognition and seizure activity in adult rats. Mol. Cell. Neurosci. 28, 347–360.

Wickersham, I.R., Sullivan, H.A., Seung, H.S., 2010. Production of glycoprotein-deleted rabies viruses for monosynaptic tracing and high-level gene expression in neurons. Nat. Protoc. 5, 595–606.